

Surface heat flow and CO₂ emissions within the Ohaaki hydrothermal field, Taupo Volcanic Zone, New Zealand

Clinton Rissmann ^{a,*}, Bruce Christenson ^b, Cynthia Werner ^c, Matthew Leybourne ^d, Jim Cole ^a, Darren Gravley ^a

^a Department of Geological Sciences, University of Canterbury, Private Bag 4800, Christchurch, New Zealand

^b National Isotope Centre, GNS-Science, PO Box 31-312, Lower Hutt, New Zealand

^c USGS, Cascades Volcano Observatory, Vancouver, WA, USA

^d GNS Science, PO Box 30-368, Lower Hutt, New Zealand

ARTICLE INFO

Article history:

Received 27 April 2011

Accepted 21 October 2011

Available online 30 October 2011

Editorial handling by R. Fuge

ABSTRACT

Carbon dioxide emissions and heat flow have been determined from the Ohaaki hydrothermal field, Taupo Volcanic Zone (TVZ), New Zealand following 20 a of production (116 MW_e). Soil CO₂ degassing was quantified with 2663 CO₂ flux measurements using the accumulation chamber method, and 2563 soil temperatures were measured and converted to equivalent heat flow (W m⁻²) using published soil temperature heat flow functions. Both CO₂ flux and heat flow were analysed statistically and then modelled using 500 sequential Gaussian simulations. Forty subsoil CO₂ gas samples were also analysed for stable C isotopes. Following 20 a of production, current CO₂ emissions equated to 111 ± 6.7 T/d. Observed heat flow was 70 ± 6.4 MW, compared with a pre-production value of 122 MW. This 52 MW reduction in surface heat flow is due to production-induced drying up of all alkali-Cl outflows (61.5 MW) and steam-heated pools (8.6 MW) within the Ohaaki West thermal area (OHW). The drying up of all alkali-Cl outflows at Ohaaki means that the soil zone is now the major natural pathway of heat release from the high-temperature reservoir. On the other hand, a net gain in thermal ground heat flow of 18 MW (from 25 MW to 43.3 ± 5 MW) at OHW is associated with permeability increases resulting from surface unit fracturing by production-induced ground subsidence. The Ohaaki East (OHE) thermal area showed no change in distribution of shallow and deep soil temperature contours despite 20 a of production, with an observed heat flow of 26.7 ± 3 MW and a CO₂ emission rate of 39 ± 3 T/d. The negligible change in the thermal status of the OHE thermal area is attributed to the low permeability of the reservoir beneath this area, which has limited production (mass extraction) and sheltered the area from the pressure decline within the main reservoir. Chemistry suggests that although alkali-Cl outflows once contributed significantly to the natural surface heat flow (~50%) they contributed little (<1%) to pre-production CO₂ emissions due to the loss of >99% of the original CO₂ content due to depressurisation and boiling as the fluids ascended to the surface. Consequently, the soil has persisted as the major (99%) pathway of CO₂ release to the atmosphere from the high temperature reservoir at Ohaaki. The CO₂ flux and heat flow surveys indicate that despite 20 a of production the variability in location, spatial extent and magnitude of CO₂ flux remains consistent with established geochemical and geophysical models of the Ohaaki Field. At both OHW and OHE carbon isotopic analyses of soil gas indicate a two-stage fractionation process for moderate-flux (>60 g m⁻² d⁻¹) sites; boiling during fluid ascent within the underlying reservoir and isotopic enrichment as CO₂ diffuses through porous media of the soil zone. For high-flux sites (>300 g m⁻² d⁻¹), the δ¹³CO₂ signature (−7.4 ± 0.3‰ OHW and −6.5 ± 0.6‰ OHE) is unaffected by near-surface (soil zone) fractionation processes and reflects the composition of the boiled magmatic CO₂ source for each respective upflow. Flux thresholds of <30 g m⁻² d⁻¹ for purely diffusive transport, between 30 and 300 g m⁻² d⁻¹ for combined diffusive-advection transport, and ≥300 g m⁻² d⁻¹ for purely advective gas transport at Ohaaki were assigned. δ¹³CO₂ values and cumulative probability plots of CO₂ flux data both identified a threshold of ~15 g m⁻² d⁻¹ by which background (atmospheric and soil respiration) CO₂ may be differentiated from hydrothermal CO₂.

© 2011 Elsevier Ltd. All rights reserved.

* Corresponding author. Tel.: +64 3 211 5201.

E-mail address: clinton.rissmann@ES.govt.nz (C. Rissmann).

1. Introduction

Over the last ~15 a, a concerted effort has been made to better characterise the magnitude of CO₂ emissions (Tonnes per day or T/d) and heat flow (MW) from volcanic and volcanic hydrothermal areas (Chioldini et al., 1998, 2005; Hernandez et al., 2000; Brombach et al., 2001; Fridriksson et al., 2006; Werner and Cardellini, 2006; and others). These studies have resulted in a better understanding of: (i) the various pathways (soil zone, hot springs, fumaroles) of heat and mass release to the atmosphere from volcanic and volcanic hydrothermal reservoirs; (ii) the relative contribution of magmatic C to the global C cycle, and; (iii) the nature of the permeability (faults, fractures, volcanic conduits) governing heat and mass release. In this paper a detailed CO₂ flux and heat flow survey is used to assess the heat and mass released from the Ohaaki hydrothermal field following 20 a of power production for municipal energy supply.

1.1. Field development and thermal activity

The Ohaaki hydrothermal field in the Taupo Volcanic Zone (TVZ), New Zealand (Figs. 1 and 2), is the site of a 116 MW_e geothermal power plant that has been producing electrical energy for the national grid for over 20 a. Prior to discharge testing in 1967, the Ohaaki West (OHW) thermal area contained an extensive range of geothermal features including the large volume (mean discharge rate of ~10 L s⁻¹) alkali–Cl outflow of the Ohaaki Pool (10 MW), ~5000 m² of steam-heated pools (8.6 MW), ~77,000 m² (25 MW) of thermal ground with temperatures >50 °C at 1.0 m depth and the seepage of a large volume (51.5 MW at ~150 kg s⁻¹) of alkali–Cl fluids from the area to the Waikato River (Dickinson, 1967; Mahon and Finlayson, 1972; Allis and Webber, 1984; Dawson, 1988; Rissmann, 2010).

Extraction during the test period (1967–1972) averaged 25,000 T/d, and without reinjection resulted in pressure decline of 1.5 MPa in deep wells (>800 m) and of 0.8 MPa in shallow (<800 m) wells (Fig. 3; Hunt and Bromley, 2000; White et al., 2005; Contact Energy, 2007). During the Test Discharge Period water levels in the large alkali–Cl Ohaaki Pool fell by 9.5 m and natural overflow ceased (Glover et al., 2000).

After completion of the 1967–1972 testing phase the Ohaaki Pool water levels rose to within 3.1 m of overflow in response to a 1.0 MPa rebound in reservoir pressure (Fig. 3; Glover et al., 2000). During this Recovery Period discharge and interference tests resulted in perturbations (up to 4 m) in the pool water level (Glover et al., 2000). Water levels did not overflow again until 1981, and then only in response to reinjection of bore water from well BR22.

In 1988, the Ohaaki Power station was commissioned and mass withdrawal increased to 45,000 T/d, with ~28,000 T/d re-injected at the reservoir margins. By 1989 the Ohaaki Pool had completely drained and in response the large pool vents were backfilled and sealed with concrete. At the same time alkali–Cl seepages to the Waikato River from the OHW thermal area were in decline. By the mid-1990s, the ~5000 m² area of steam-heated pools had dried up in response to pressure-induced lowering of local water tables (Hunt and Bromley, 2000). By 2000 reservoir pressure had declined by 2.5 MPa (25 bar; Fig. 3), and mass withdrawal from the reservoir had caused significant (>2.5 m) ground subsidence, which resulted in local fissuring of the cap rock at OHW and development of new areas of thermal ground (Hunt and Bromley, 2000). By 2000 on-going ground subsidence at OHW caused the submergence of former alkali–Cl seepage sites and subsequent inundation by the Waikato River.

Hunt and Bromley (2000) reported little change in surface thermal activity at the Ohaaki East (OHE) thermal area following 12 a

of production. Ohaaki East is characterised by ~23,000 m² of thermal ground with no alkali–Cl outflows, a few moderately sized steam-heated pools and numerous small boiling mud pots (<1000 m²) (Fig. 2; Dickinson, 1967; Mahon and Finlayson, 1972; Allis and Webber, 1984; Dawson, 1988). Dickinson (1967) provided an estimate of ~0.2 MW for the steam heat pools of OHE but did not undertake a measure of the heat flow associated with thermal ground. Pre-production thermal activity at BR6 was negligible, with only one small area (<400 m²) of soil temperatures in excess of 50 °C at 1.0 m depth, and no steam-heated pools or alkali–Cl outflows (Allis and Webber, 1984; Dawson, 1988). Since production began the small area of elevated temperatures has disappeared.

1.2. Scope of this study

Prior to discharge testing, Dickinson (1967) conducted a detailed heat flow assessment of OHW but not of OHE. Since then no new heat flow assessment based on direct measurement has been undertaken. In this study detailed CO₂ flux and heat flow surveys were used to quantify heat flow and CO₂ emissions and to assess production-induced changes in surface thermal activity at the Ohaaki Field. The relationship between geochemical models that assess deep reservoir conditions and CO₂ flux were examined. Dominant heat and mass transfer flow paths were characterised and stable C isotopes used to examine the origins of CO₂ and characterise its transport from the deep reservoir to the surface. A detailed assessment of the structural controls over surface thermal activity at Ohaaki is presented in Rissmann et al. (2011).

2. Study area

2.1. Regional geology

The Ohaaki Field is located within the (~720 km²) Reporoa Basin, along the eastern boundary of the TVZ (Fig. 1). The TVZ is a 250 km NE-trending zone of mainly andesitic to rhyolitic arc/back arc volcanism, within continental crust of the central North Island, New Zealand (Cole, 1990). TVZ volcanism evolved over the past 1.6 Ma and is spatially coincident with a narrow (15–40 km wide) zone of active crustal extension known as the Taupo Rift (Wilson et al., 1995). Volcanism and rifting in the TVZ, which formed in association with subduction of the Pacific Plate beneath the North Island, produced crustal thinning and high average geothermal heat flow (~700 mW m⁻²) (Bibby et al., 1995; Stratford and Stern, 2006; Nicol et al., 2007). Heat flow in the TVZ is highly variable and is focused within 23 main geothermal fields, one of which is the Ohaaki Field (inset Fig. 1).

2.2. Ohaaki reservoir

The Ohaaki hot water reservoir, as defined by the area of low resistivity (i.e., <10 mΩ), covers 12.7 km², has high non-condensable gas concentrations causing boiling at depths >1500 m and has a maximum reservoir temperature of 310 °C (Grant, 1977; Hedenquist, 1990; Giggenbach, 1995; Christenson et al., 2002). Two major high-temperature plumes enter the reservoir through permeable pathways associated with the Ohaaki Fault in the NW (West Bank upflow) and an unnamed normal fault in the SE (East Bank upflow) (Figs. 2 and 4; Christenson et al., 2002; Rae et al., 2007). The East Bank upflow has a more magmatic character than the West Bank with significantly higher non-condensable gas concentrations and higher B, but with lower Cl (Christenson et al., 2002). Compositional differences are attributed to two, shallowly emplaced (≥ 4.5 km), intrusive bodies – the East Bank intrusive is

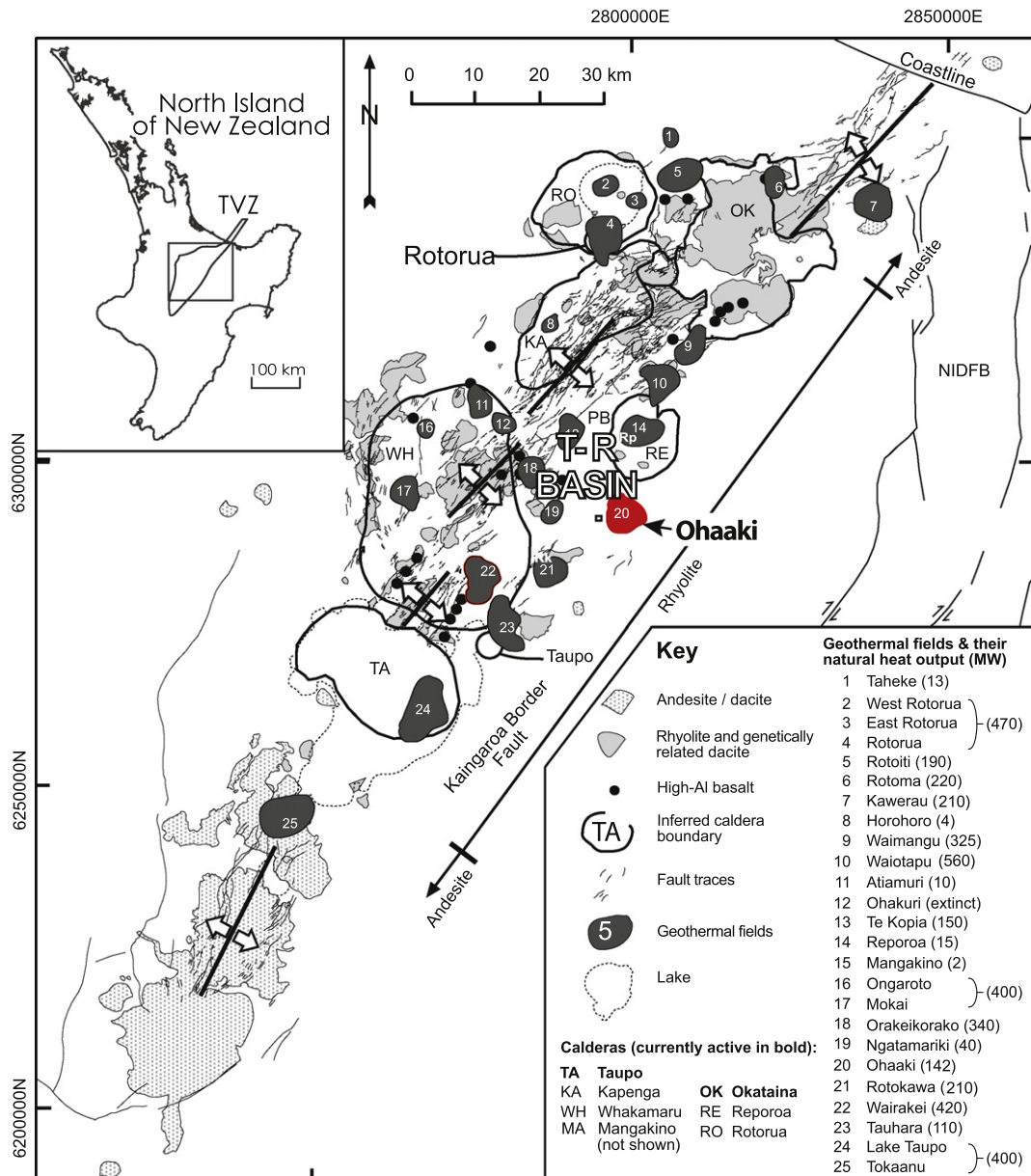


Fig. 1. Map of the Taupo Volcanic Zone showing the distribution of geothermal systems, defined by the presence of low-resistivity zones ($<30\ \Omega\text{ m}$) in relation to rift architecture, major volcanic rock types and caldera boundaries (modified from Rowland and Sibson, 2004). Where: T-R Basin = the Taupo Reporoa Basin; NIDFB = North Island Dextral Fault Belt, and; the Ohaaki hydrothermal field is in red. Major towns, Taupo and Rotorua, are labelled. The Wairakei field is outlined in red and lies ~20 km SW of Ohaaki. (For interpretation of the references to colour in this figure legend, the reader is referred to the web version of this article.)

younger and thought to be emplaced at a shallower level (Christenson et al., 2002). Although distinct from one another, the fluid chemistry of each upwelling is characteristically volcanic–magmatic or ‘arc-type’, consistent with high non-condensable gas concentrations and large N_2/Ar ratios (Fig. 2; Christenson et al., 2002).

The stratigraphy of the Ohaaki reservoir consists of: (1) Mesozoic greywacke basement underlying the field; (2) pre-330 ka volcanic-sedimentary strata of the Waikora and Tahorakuri Formations that directly overlie the basement; (3) the 330 ka Rangitaiki Ignimbrite that overlies these, and; (4) post-330 ka volcanic-sedimentary infill that includes the poorly permeable (0.03–0.5 mD) Huka Falls Formation (HFF) caprock (Fig. 4). The greywacke basement is block-faulted over four major NE-trending (arc-parallel) and steeply dipping normal faults. The basement is displaced from ~700 mRSL (relative sea level) in the SE sector to ~2100 mRSL in the NW over a lateral distance of ~2.8 km (Wood

et al., 2001; Rae et al., 2007). The majority of this relief (1400 m) is accommodated by major fault scarps of the Ohaaki Fault Zone and Broadlands Fault Zone, which occur within the NW and SE sectors of the field, respectively (Figs. 2 and 4).

The reservoir overlying the greywacke basement is a complex assemblage of pre-330 ka volcaniclastic units and post-330 ka volcanic domes, intercalated with pyroclastic deposits from large caldera-forming eruptions to the west (Fig. 4). With the exception of the fractured and brecciated apex of each dome, lava flows tend to inhibit vertical fluid movement (Henrys and Hochstein, 1990; Hedenquist, 1990; Rissmann et al., 2011). Pyroclastic flow deposits and porous volcaniclastic units (i.e., the Rangitaiki Ignimbrite, Rauwhiri Breccia and the shallow Waiora Formation) act as permeable aquifers through which ascending alkali–Cl hot waters outflow laterally (Hedenquist, 1990; Wood, 1994). The Waiora Formation forms an important shallow alkali–Cl aquifer, which in places

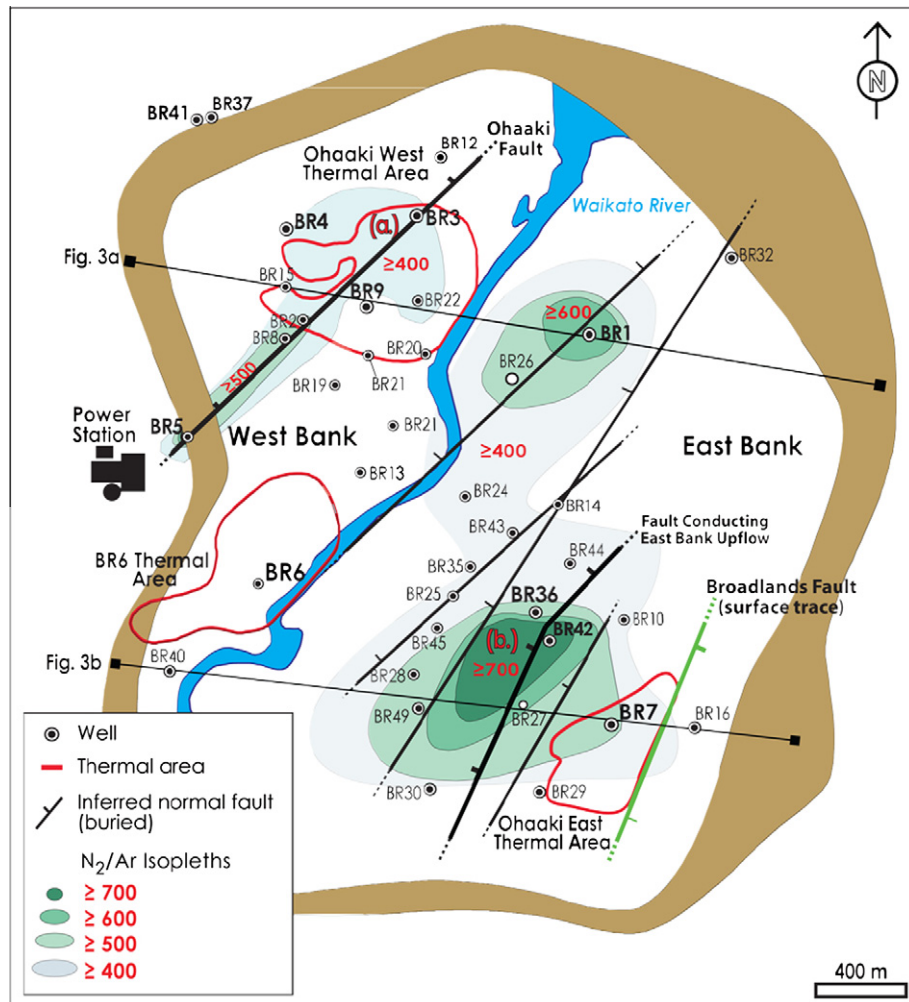


Fig. 2. Plan view of the Ohaaki Field including resistivity boundary, inferred deep-seated normal faults, N₂/Ar isopleths and location of major thermal areas (from Wood et al., 2001; Christenson et al., 2002). N₂/Ar isopleths denote the major hydrothermal upflows of the field. The subsurface expression of the Ohaaki Fault is depicted in the upper left of the field where it conducts the West Bank upflow from depth up into the Ohaaki Rhyolite dome (Christenson et al., 2002; Rae et al., 2007; Rissmann et al., 2011). The East Bank upflow is channelled through a large deep-seated normal fault in the SE sector of the field. The surface trace (in green) of the Broadlands Fault borders the eastern margin of the Ohaaki East thermal area, transects the Broadlands Dacite dome and governs the occurrence of surface thermal activity (Rissmann et al., 2011). The location of major thermal areas, Ohaaki West (OHW) and Ohaaki East (OHE), and low temperature BR6 thermal area are shown. Thermal areas are delineated by 1.0 m depth temperatures $\geq 25^{\circ}\text{C}$, after Allis and Webber (1984) and this study. A large seepage (150 kg s^{-1} and $\sim 51.5 \text{ MW}$) of alkali–Cl hot water once discharged into the Waikato River from the Ohaaki West thermal area. The lines of cross-section for Fig. 4a and b are also displayed. (For interpretation of the references to colour in this figure legend, the reader is referred to the web version of this article.)

directly underlies the HFF (Wood, 1994). The reservoir is capped by the poorly permeable mudstones of the HFF, which at Ohaaki are especially thick (Fig. 5; mean of $\sim 220 \text{ m}$ and maximum thickness of 440 m; Contact Energy, 2007).

2.3. Thermal areas

All three thermal areas at Ohaaki occur above the apices of buried or partially emergent lava domes (Figs. 4 and 5). Recently, Rissmann et al. (2011) assessed the geology and fluid flow regimes of both the OHW and OHE thermal areas. The distinct horseshoe shaped distribution of thermal activity at OHW about the apex of the extinct Ohaaki Rhyolite dome is due to the ascent of hydrothermal fluids through remnant permeability structures (dyke margins, conduit shear zones and/or eruptive vents) associated with dome growth and eruption (Rissmann et al., 2011). At OHE the pattern of thermal activity has been attributed to the presence of a channel-barrier fluid flow system associated with the transection of the Broadlands Dacite dome by the Broadlands Fault (Rissmann

et al., 2011). In both thermal areas the apices of lava domes allow underlying fluids to bypass the poorly permeable HFF cap rock and discharge at the surface (Rissmann et al., 2011).

3. Methods

3.1. Field measurement of CO₂ flux and soil temperature

Soil CO₂ fluxes and shallow soil temperatures (0.15 m depth) were measured at 2663 and 2563 locations, respectively, across areas of thermal and non-thermal ground on the West and East Banks of the Ohaaki Field (Fig. 6). All flux and soil temperature measurements were conducted at least 3 days after light rainfall, and 5 days after heavy rainfall, during the summer months (December–March) of 2006–2008. The CO₂ fluxes were measured using a West Systems accumulation chamber (using the recommendations of Welles et al., 2001) and a LICOR LI-820 infrared gas analyser.

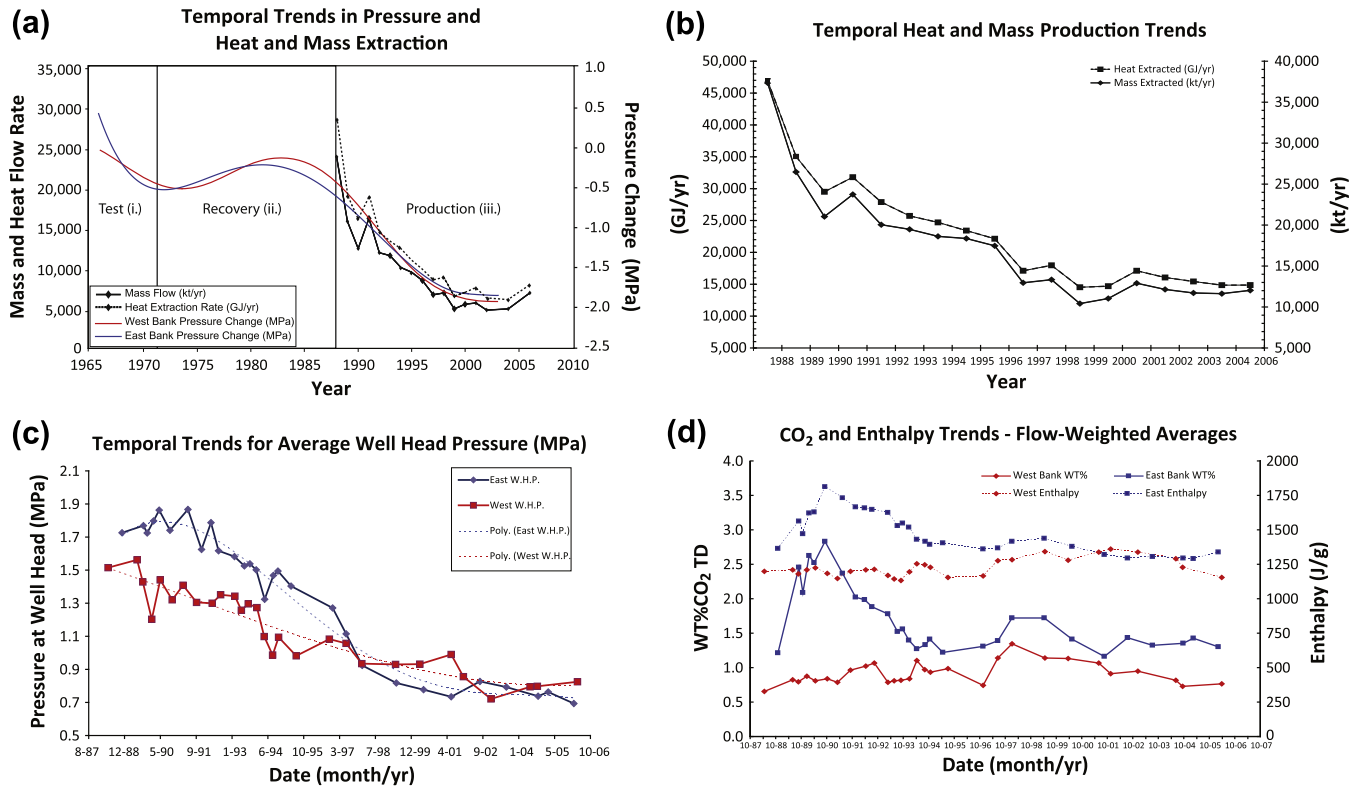


Fig. 3. Conceptual diagrams displaying the temporal evolution of physical and chemical characteristics of the Ohaaki reservoir in response to production. (a) Characteristic trends in reservoir pressure, heat and mass flow, at Ohaaki due to development. Pressure changes are based on production well data for the deep reservoir (≥ 500 m below ground level (b.g.l.)), where: (i) Test Discharge Period, (ii) Recovery Period, and (iii) Production Period. (b) Enlargement of the temporal trend in heat and mass extraction from the Ohaaki reservoir. An initial steep decline in heat and mass extraction in the first 2 years of production is followed by a more gradual decline and the eventual flattening of the curve as the system appears to approach a steady state. (c) Temporal trend of average well head pressure (WHP). A sharp decline in WHP over the first 10 a of production is followed by a more gradual decline and eventual flattening for both East- and West Bank reservoirs and appears to approach a steady state. (d) Trends in weight% CO₂ and enthalpy of production fluids from West and East Bank reservoirs. Flow weighted averages for the East Bank reservoir display an initial spike in wt.% CO₂ and enthalpy in response to production of the reservoir and then decline sharply before flattening out. West Bank production fluids do not show any spike in wt.% CO₂ or enthalpy and vary little over the time period displayed. All data from Contact Energy (2007).

At all flux sites soil temperature were measured at a depth of 0.15 m, typically within 0.2 m of the accumulation chamber footprint, using a Yokogawa TX-10 digital thermometer and a K-type thermocouple (measurement accuracy was ± 0.3 °C). Additional measurements of the soil temperature gradient were made for all sites where soil temperature exceeded boiling point at 0.15 m. This was accomplished by measuring soil temperature incrementally at depths of 1 cm, 2.5 cm, 5 cm, 10 cm and 15 cm. Within OHE 53, 1.0 m-depth, temperature readings were conducted to assess changes in the distribution and/or magnitude of soil temperatures mapped in earlier surveys (i.e., Allis and Webber, 1984; Hunt and Graham, 1997). Global Positioning System (GPS) co-ordinates, CO₂ flux and soil temperatures were recorded at each site, whereas barometric pressure and ambient air temperature were recorded at the start of each day and after each set of 25 consecutive measurements.

The survey focused initially on areas of active thermal ground within OHW and OHE, and extended to cover all areas of historically documented thermal ground (subsoil temperatures ≥ 25 °C above ambient at 1.0 m depth), concluding with a survey of peripheral non-thermal ground surrounding each thermal area. (Hereafter, subsoil temperature refers to depths ≥ 50 cm within the soil zone). Within the BR6 thermal area, flux and temperature measurements were conducted at 15 m intervals along 12 transects (Fig. 6). Only three small areas (< 16 m² at ≤ 200 g m⁻² d⁻¹) of moderately elevated flux were detected in this area, and a more detailed survey was not undertaken. On the East Bank flux and temperature measurements were conducted at 15–25 m intervals

along 26 transects in areas that lack surface thermal activity (i.e., no subsoil temperature anomaly or surface thermal features), but for which geochemical data indicate upwelling of high temperature plumes at depth (Figs. 2 and 6; Christenson et al., 2002).

The sampling design within OHW and OHE was based on a simple random sampling pattern with an adaptive sampling component, whereby adjustments to the sampling density were made in areas of changing CO₂ flux, and/or soil temperature. Cumulative probability plots of the flux data indicate that the background CO₂ flux was 0.5 ppm s⁻¹ (or ~ 15 g m⁻² d⁻¹) and was confirmed by $\delta^{13}\text{C}$ -CO₂ values of sampled soil gas (see Sections 4.4 and 5.4). Adaptive sampling was triggered whenever the CO₂ flux exceeded the background flux and/or when soil temperatures at 0.15 m exceeded ambient air temperature. At these sites the extent of the anomaly was characterised by sampling directly N, S, E and W of the initial sample location. Sample density ranged between 5 and 15 m in areas of anomalous flux and/or soil temperature, resulting in a higher sampling density or clustering of sampling points within and about the anomaly. A return to background CO₂ flux values and/or soil temperatures governed the return to 'normal' sampling densities (i.e., every ~ 25 m) and the simple random sampling pattern.

Adaptive sampling was implemented to improve accurate representation of the spatial variability of CO₂ flux and soil temperature, and to provide a representative data set for estimating total emissions and heat flow from each thermal area. Potential problems from the higher sample densities (i.e., clustering) within areas of anomalous flux and/or soil temperature include bias in population statistics (Goovaerts, 1997; Deutsch and Journel, 1998). Therefore,

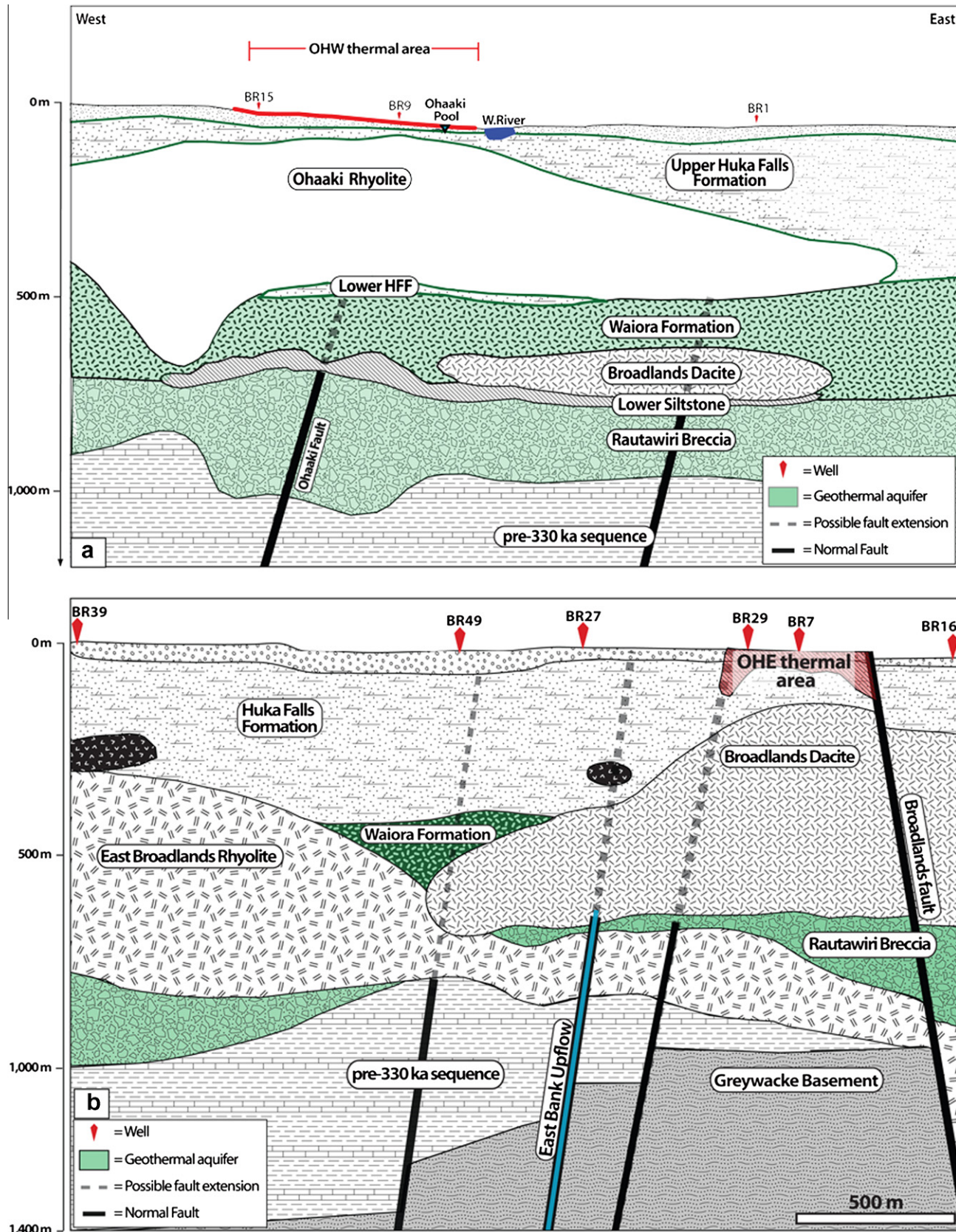


Fig. 4. East–west cross-sections through the Ohaaki reservoir (modified from Milich et al., 2010). (a) Cross section through the NW sector of the field and the OHW thermal area. (b) Cross section through the SE sector of the field and the OHE thermal area. Fault locations are idealised and not to scale.

it was necessary to debiase or decluster the data by weighting each datum according to its proximity to surrounding data. Declustering

does not change the value of the sampled variable, only the influence of each sample (Journel, 1994; Goovaerts, 1997).

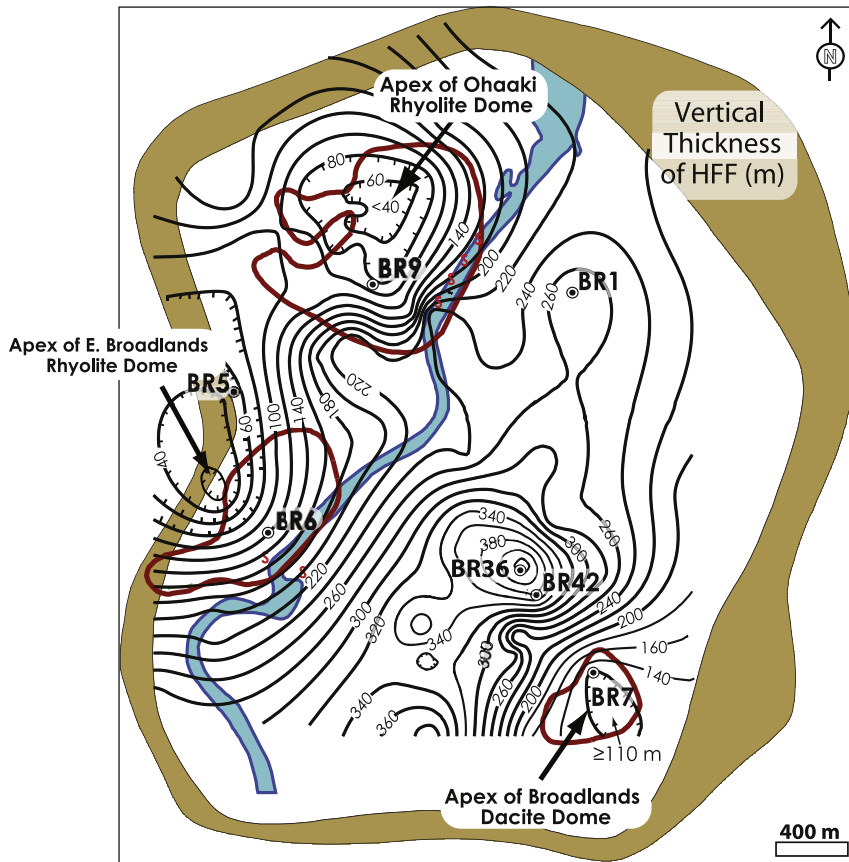


Fig. 5. Contour plot of the combined vertical thickness of the Huka Falls Formation (m). Note the thinning of the HFF and the occurrence of thermal areas above the apices of the Ohaaki Rhyolite dome in the NW, the Broadlands Dacite dome in the SE, and the East Broadlands Rhyolite in the SW.

3.2. Data treatment for CO₂ emissions calculation

The CO₂ flux and soil temperature data sets were declustered for OHW and OHE using the cell declustering algorithm DECLUS within the software toolbox WinGislib (Deutsch and Journel, 1998). Each declustered data set was modelled using the sequential Gaussian simulations (sGs) algorithm (SGSIM), within WinGislib. The main data analysis steps for each thermal area were: (i) normalisation (n-score) of the declustered data; (ii) computation of the experimental variogram of n-score values; (iii) definition of the variogram model for each data set; (iv) perform 500 sGs of the normal scored data, and; (v) back-transformation of the simulated normal values into simulated values of the original variable (CO₂ flux) (Cardellini et al., 2003; Chiodini et al., 2004).

Post-processing of the 500 flux grid realisations included: (i) computation of mean flux and the probability of high and low fluxes at each location; (ii) generation of 2D pixel plots of CO₂ flux across the field surface; (iii) calculation of emission rates (T/d) for each realisation by summing the simulated flux across the grid and multiplying by the grid area, and; (iv) calculation of average and standard deviations of the emission rates from the 500 flux realisations conducted for each grid area.

3.3. Heat flow estimates

The measured shallow soil temperatures were converted to equivalent heat flow values using the empirical equations of Dawson (1964) and Hochstein and Bromley (2005). These authors measured shallow soil temperatures, boiling point depth, and surface heat flow from areas of thermal ground within the nearby Wairakei geothermal

field, ~20 km SW of Ohaaki (Fig. 1). In both studies surface heat flow was measured using a water-filled calorimeter (see Dawson and Dickinson, 1970; Hochstein and Bromley, 2005). Empirical power law functions were derived to convert shallow soil temperatures to equivalent heat flow values (Eqs. (1) and (2)).

It is suggested that differences between the heat flow characteristics between Wairakei and Ohaaki are likely to be small, given the similar geological and climatic setting and the development of thermal soils at both fields within the same parent material – the Taupo Pumice Alluvium. For areas where soil temperatures did not reach the boiling point within 0.15 m of the surface heat flow was calculated using Dawson's (1964) equation:

$$H_s = 5.2 \times 10^{-6} T_{15}^4 \quad (1)$$

where H_s is heat flow (in W m⁻²) at the soil surface and T_{15} is the soil temperature at 0.15 m in °C. For high-temperature sites where boiling occurs within 0.15 m of the surface, Hochstein and Bromley's (2005) equation was applied:

$$H_s = a \left(\frac{z_{BP}}{z_0} \right)^{-b} \quad (2)$$

where $a = 185 \text{ W m}^{-2}$, $b = 0.757$, z_{BP} is the depth of boiling in m, and z_0 denotes unit depth (1 m). Particular care was taken to accurately measure boiling point depth, as major gains in heat flow occur with only slight increases in soil temperature once boiling occurs (Dawson, 1964; Hochstein and Bromley, 2005). Eq. (1) was applied to 2241 measurements, and Eq. (2) to 322 measurements. The spatial distribution of heat flow (MW) was then modelled for both thermal areas through 500 sGs realisations using the method as described above for soil CO₂ flux. Using empirical power law functions to

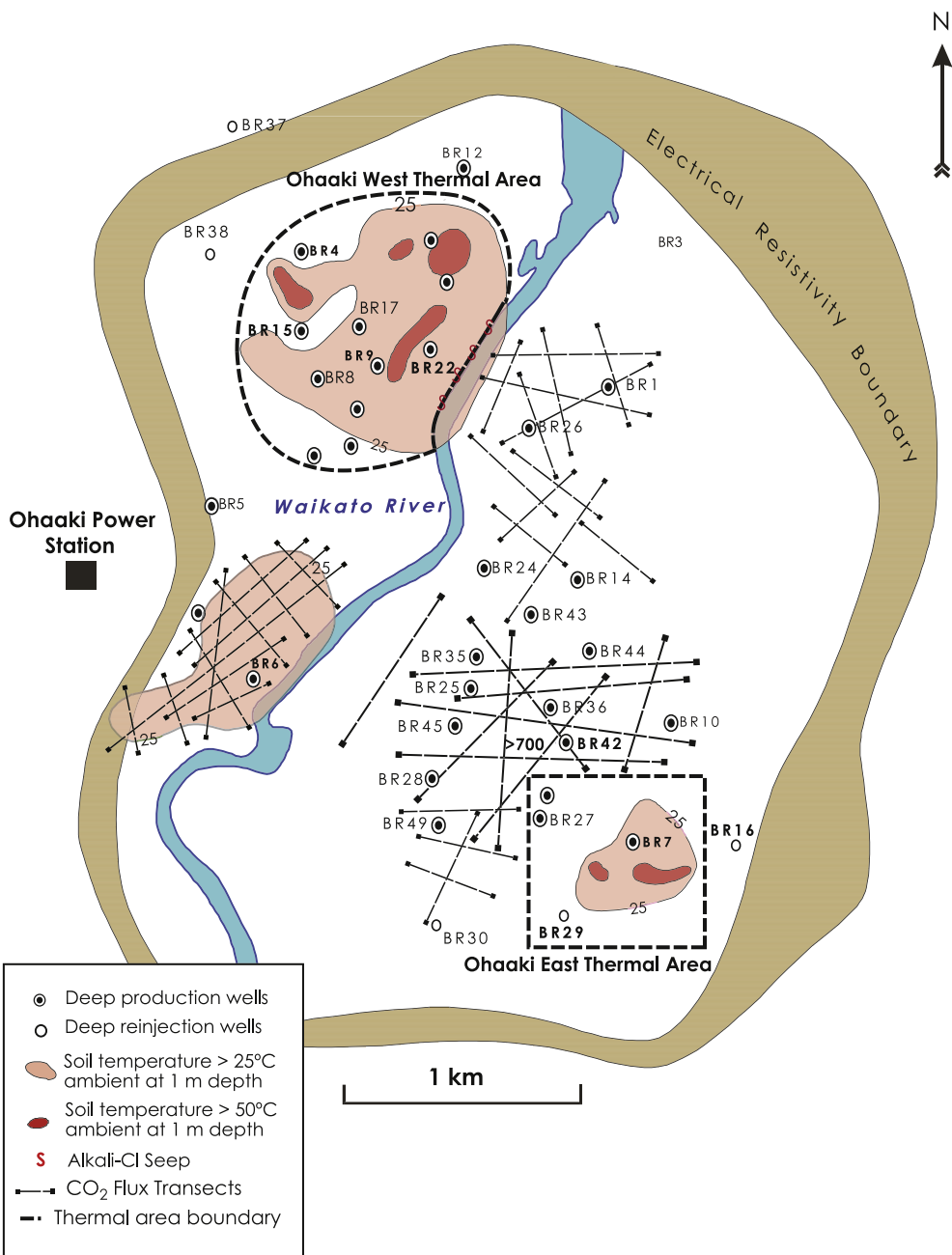


Fig. 6. Map of sampling locations within the Ohaaki Field. Boxed and dashed areas delimit the extent of the intensive CO₂ flux and soil temperature survey. Soil temperature and CO₂ flux transects are depicted for the BR6 thermal area and the East Bank reservoir.

describe thermal ground heat flow enabled a direct comparison with the heat flow values of Dickinson (1967), who also utilised similar methods to quantify the pre-production heat flow from the OHW thermal area more than 40 a ago.

3.4. Calculation of mass transport of steam

By assuming that the heat flow of each thermal area is a manifestation of water vapour (hereafter referred to as steam) transported from the underlying reservoir to the surface, the mass flow of steam through soil, $F_{\text{stm,HF}}$ in kg s⁻¹, was computed using the method of Fridriksson et al. (2006):

$$F_{\text{stm,HF}} = \frac{H_s}{(h_{s,98.7^\circ\text{C}} - h_{w,tr})} \quad (3)$$

where H_s is the measured thermal ground heat flow (in W), $h_{s,98.7^\circ\text{C}}$ is the enthalpy of steam at 98.7 °C (boiling point at Ohaaki) and $h_{w,tr}$ is the enthalpy of water at 20 °C, which was the mean air temperature during the survey periods (2673.7 kJ kg⁻¹ and 83.9 kJ kg⁻¹, respectively).

3.5. Carbon isotopes of soil CO₂ flux

Forty subsoil gas samples were collected at 0.5 m depth from sites within OHW and OHE for determination of $\delta^{13}\text{CO}_2$. Flux and soil temperature (0.15 m) were measured at each site prior to sample collection. The gases were drawn under vacuum into Tedlar bags, which were purged three times with soil gas before collecting. To characterise the study area, sites were sampled throughout the range of flux and soil temperature values. Stable C-isotope

ratios of CO₂ were determined by Iso-Trace Ltd., Dunedin, New Zealand, and the National Isotope Centre, GNS Science, Lower Hutt, New Zealand. Results are presented using δ notation as ‰ deviations from the VPDB standard.

4. Results

4.1. Diffuse fluxes and soil temperature

Measured CO₂ fluxes ranged from undetectable ($<3\text{ g m}^{-2}\text{ d}^{-1}$) to $27,518\text{ g m}^{-2}\text{ d}^{-1}$. The analyser upper detection limit (i.e., 20,000 ppm s⁻¹) was exceeded five times within OHW indicating localised fluxes in excess of $32,000\text{ g m}^{-2}\text{ d}^{-1}$. The arithmetic and declustered means of CO₂ flux for the OHW and OHE data sets were 157 and $122\text{ g m}^{-2}\text{ d}^{-1}$, and 86 and $77\text{ g m}^{-2}\text{ d}^{-1}$, respectively. The coefficients of variation for the flux data collected from OHW and OHE were 6.1 and 5.7, respectively, where a CV > 1 is consistent with a non-normal (positively skewed) approximately log-normal population distribution, as is evident in the histograms of CO₂ flux (Fig. 7).

Within OHW, 16% of the fluxes exceeded $100\text{ g m}^{-2}\text{ d}^{-1}$, compared with 25% within OHE. However, 40 measurements exceeded $1000\text{ g m}^{-2}\text{ d}^{-1}$ at OHW, compared with only 11 measurements $>1000\text{ g m}^{-2}\text{ d}^{-1}$ within OHE. The CO₂ emissions along transects across the BR6 thermal area were negligible and only three small areas ($\leq 4\text{ m}^2$) had CO₂ fluxes (maximum of $200\text{ g m}^{-2}\text{ d}^{-1}$) greater than background. On the East Bank, CO₂ fluxes and shallow soil

temperatures along transects across areas of deep upwelling were at or below background values.

Shallow (0.15 m) soil temperatures across the Ohaaki Field ranged from 10 °C to boiling. Significant gas discharge ($>100\text{ g m}^{-2}\text{ d}^{-1}$) through cold ground was observed at both OHW and OHE. These appear to result from steam quenching by cold meteoric groundwater. At these sites there was no correlation between 0.15 m soil temperatures and CO₂ flux ($R^2 = 0.08$). For high temperature sites ($T > 50\text{ }^\circ\text{C}$) there was a better, albeit weak, correlation between soil temperature and fluxes (i.e., $R^2 = 0.45$ and 0.39 for the OHW and OHE thermal areas, respectively), indicating less decoupling of steam (heat flow) flux from CO₂ for high temperature sites.

A cumulative probability plot of the entire flux data set displays major inflections at $\sim 15\text{ g m}^{-2}\text{ d}^{-1}$, $30\text{ g m}^{-2}\text{ d}^{-1}$, $900\text{ g m}^{-2}\text{ d}^{-1}$ and $2300\text{ g m}^{-2}\text{ d}^{-1}$ defining five possible flux populations. The inflection at $15\text{ g m}^{-2}\text{ d}^{-1}$ is interpreted as the threshold by which background (atmospheric and soil respiration CO₂) and hydrothermal populations may be differentiated (Fig. 8). A background of $15\text{ g m}^{-2}\text{ d}^{-1}$ is supported by $\delta^{13}\text{C}-\text{CO}_2$ isotopic data (see Section 5.4.).

4.2. Sequential Gaussian simulation

A good fit between the experimental (flux and temperature data variograms) and model variograms was obtained for each flux population with nugget values of 0.56 and 0.46, both sill equal to 1,

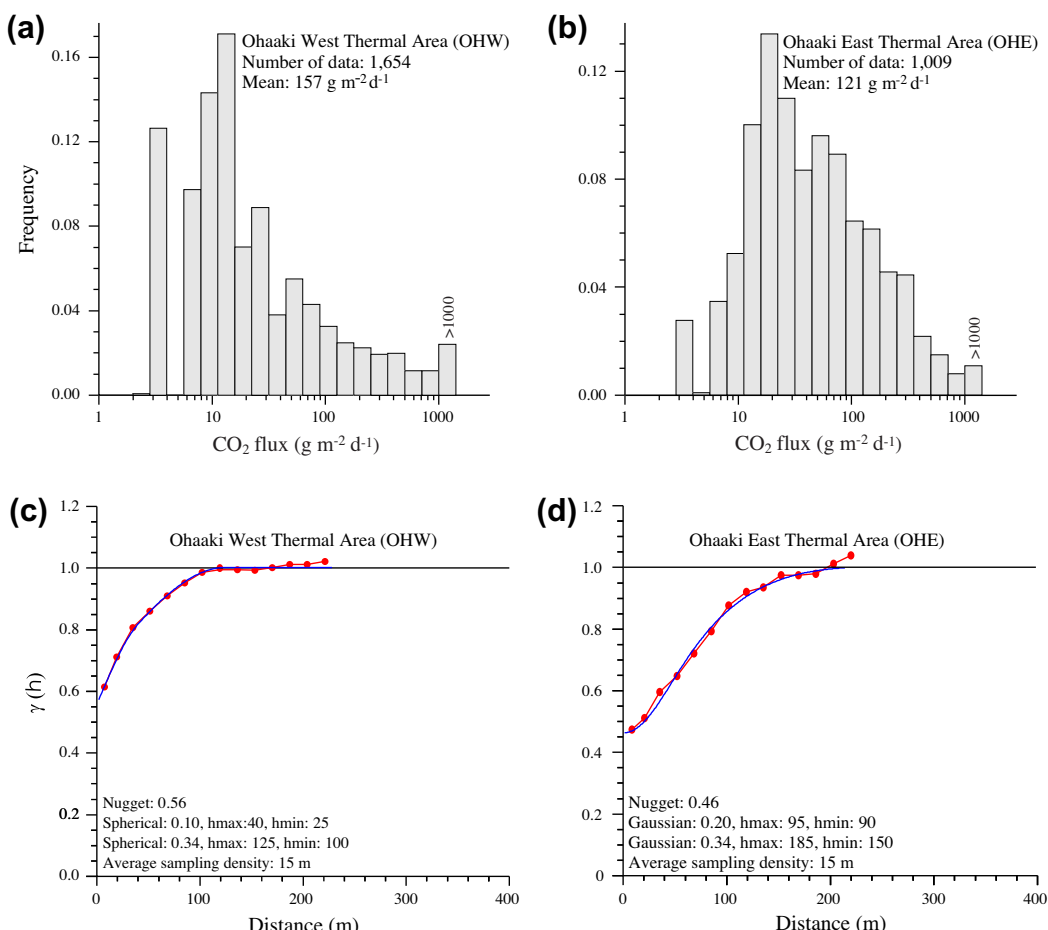


Fig. 7. (a and b) Frequency histograms showing CO₂ flux populations and statistics for the OHW and OHE thermal areas. (c and d) Experimental (red lines) and model (dark blue lines) semivariograms for CO₂ measurements within the OHW and OHE thermal areas. (For interpretation of the references to colour in this figure legend, the reader is referred to the web version of this article.)

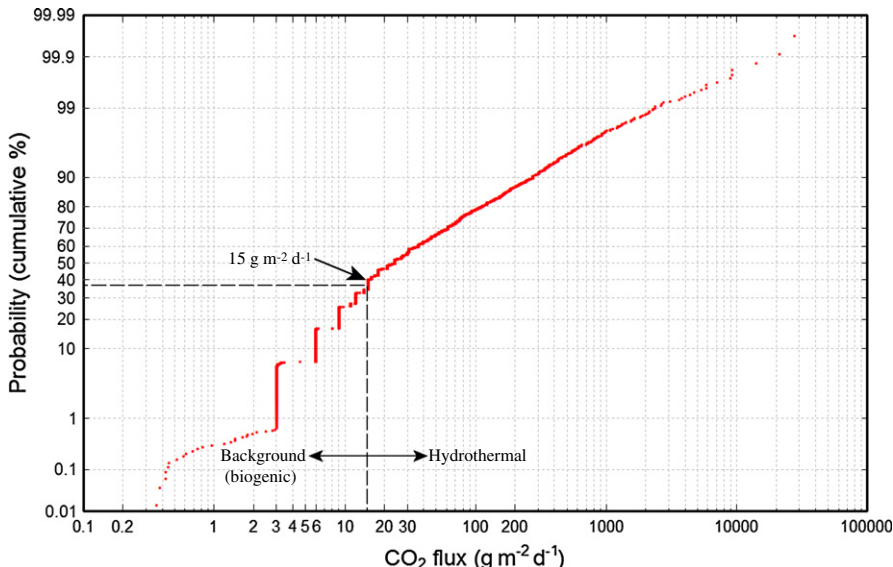


Fig. 8. Cumulative probability plot of CO_2 flux ($\text{g m}^{-2} \text{d}^{-1}$) data for the entire Ohaaki Field (data from thermal and non-thermal areas included). A single arrow identifies a major inflection at a CO_2 flux of $\sim 15 \text{ m}^{-2} \text{ d}^{-1}$, which is interpreted as the threshold between background CO_2 flux derived predominantly from soil respiration and the much more significant hydrothermal CO_2 component.

and effective ranges of 120 m and 200 m, respectively (Fig. 7). Similarly, model variograms were fitted for heat flow data sets by superposition of exponential and Gaussian models with nugget values of 0.20 and 0.21, sill of 1.0, and effective ranges of approximately 110 m and 130 m, for OHW and OHE, respectively. The results of the 500 simulations are depicted in Figs. 9 and 10 for OHW and OHE, respectively. These models illustrate that diffuse degassing and anomalous heat flow extended over hundreds of metres in both thermal areas.

4.3. Estimates of CO_2 emissions and heat flow through soil

The mean emission rates from the 500 simulations equated to $72 \pm 6 \text{ T/d}$ and $39 \pm 3 \text{ T/d}$ for OHW and OHE, respectively with a total emission of $111 \pm 6.7 \text{ T/d}$. Heat flow at OHW and OHE, estimated using Eqs. (1) and (2), ranged from 0.2 to 2460 W m^{-2} , with mean heat flow values of 44 W m^{-2} and 38 W m^{-2} , respectively. The average heat flow calculated from the 500 simulations equate to $43 \pm 5 \text{ MW}$ and $27 \pm 4 \text{ MW}$ for OHW and OHE, respectively, with a combined total of $70 \pm 6.4 \text{ MW}$ (Table 1). Assuming that steam condensation within the soil is the dominant heat transfer mechanism, the mass flow of steam to each area equates to $1430 \pm 155 \text{ T/d}$ and $880 \pm 115 \text{ T/d}$, respectively (Eq. (3)).

4.4. Carbon isotope composition of soil CO_2

Carbon isotope values of CO_2 range from $-2.4\text{\textperthousand}$ to $-16.6\text{\textperthousand}$ within OHW and OHE (Table 2). For high temperature ($\geq 45^\circ\text{C}$ at 0.15 m), high flux ($\geq 300 \text{ g m}^{-2} \text{ d}^{-1}$) sites, however, $\delta^{13}\text{CO}_2$ values varied only slightly around mean values of $-7.4 \pm 0.3\text{\textperthousand}$ and $-6.5 \pm 0.6\text{\textperthousand}$ for OHW and OHE, respectively. These means are similar to the mean bleed-line compositions of the West ($-7.5 \pm 1.1\text{\textperthousand}$) and East Bank ($-6.8 \pm 0.7\text{\textperthousand}$) reservoirs, respectively (Christenson et al., 2002).

The $\delta^{13}\text{CO}_2$ variability is greater for low temperature ($< 40^\circ\text{C}$), low flux ($< 300 \text{ g m}^{-2} \text{ d}^{-1}$) sites compared to high flux sites. Values range from $-6.7\text{\textperthousand}$ to $-10.9\text{\textperthousand}$ and $-2.4\text{\textperthousand}$ to $-16.6\text{\textperthousand}$, and have mean isotopic compositions of $-9.0 \pm 2.3\text{\textperthousand}$ and $-5.2 \pm 1.8\text{\textperthousand}$ for OHW and OHE, respectively. Within OHE, all low temperature ($17\text{--}40^\circ\text{C}$), low to moderate flux ($> 15\text{--}300 \text{ g m}^{-2} \text{ d}^{-1}$) sites exhibit

relatively isotopically enriched $\delta^{13}\text{CO}_2$ values of $-6.2\text{\textperthousand}$ to $-2.4\text{\textperthousand}$, but this was not observed at the low or moderate flux sites within OHW. However, no gas samples were collected over the range $100\text{--}300 \text{ g m}^{-2} \text{ d}^{-1}$ for OHW, resulting in an unintended sampling bias towards either high- or low-flux sites. Within all three thermal areas depleted isotopic signatures ($-16.6\text{\textperthousand}$ to $-9.0\text{\textperthousand}$) occurred at low flux ($\leq 15 \text{ g m}^{-2} \text{ d}^{-1}$), low temperature ($< 40^\circ\text{C}$) sites with dense stands of non-thermal vegetation.

5. Discussion

5.1. Changes in surface thermal activity and pre-production heat flow

Calculations show a decline of $\sim 70 \text{ MW}$ in natural surface heat flow from OHW since production testing began in 1967. This large decrease reflects the drying up of steam-heated pools (8.6 MW) and alkali-Cl outflows (both Ohaaki Pool and seepage; 61.5 MW) from the OHW thermal area (Table 1). The rapid decline in the Ohaaki Pool and seepages to the Waikato River is consistent with the reported sensitivity of liquid-dominated outflows to reservoir pressure decline (Sorey et al., 1980; Grant et al., 1982).

On the other hand, comparison of heat flow values for thermal ground indicate an 18 MW increase from 25 MW to $43 \pm 5 \text{ MW}$ since 1964. A post-production increase in thermal ground heat flow is supported by repeat thermal infrared (TIR) surveys flown in 1988 and in 1998 that showed a marked increase in the extent of thermal ground and magnitude of surface heat flow in response to production induced ground subsidence and fracturing of the HFF cap rock (Hunt and Bromley, 2000). Unfortunately, vegetative screening and steam clouds precluded attempts to accurately quantify the heat-flow increases evident in TIR images (Hunt and Bromley, 2000). Since 1998, tension fractures have continued to form in response to on-going ground subsidence increasing the permeability of surface units, enabling a greater portion of steam and hydrothermal gases to ascend from the underlying reservoir to the surface.

Fracturing is especially notable within the large area of thermal ground adjacent to well BR9 where numerous fractures, developed along the shoulder of a major subsidence bowl (i.e., within a zone of maximum tensional strain), appear to control the extent and spatial orientation of thermal ground and CO_2 emissions

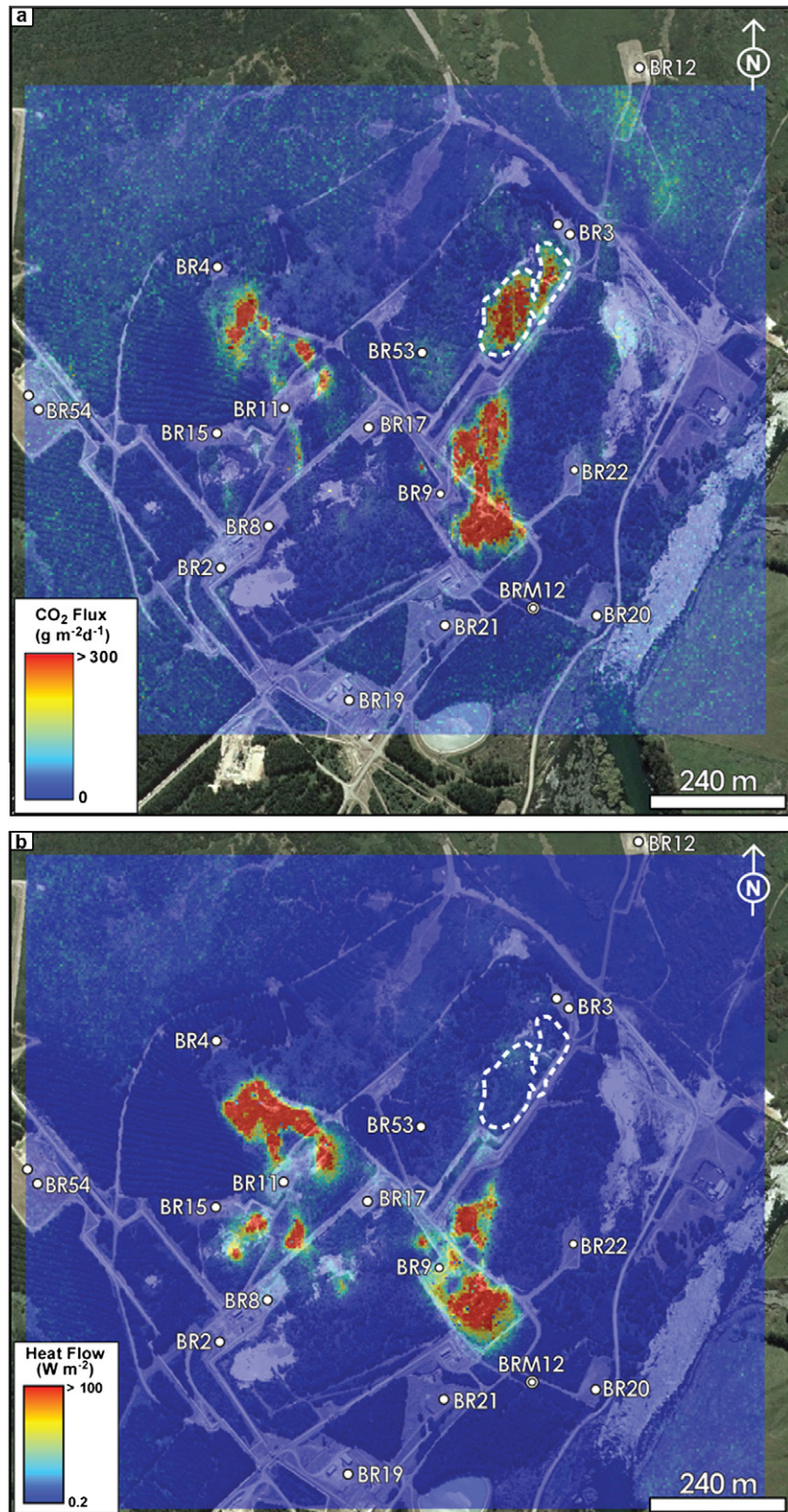


Fig. 9. (a) Pixel plot of sequential Gaussian simulations of diffuse CO₂ flux of the OHW thermal area. (b) Pixel plot of sequential Gaussian simulations of thermal ground heat flow within the OHW thermal area. Note: (i) absence of heat flow anomaly despite elevated CO₂ flux SW of well BR3, and; (ii) the anomalous CO₂ flux and heat flow associated with the large tract of thermal ground adjacent to well BR9.

(Fig. 11). This large tract of thermal ground appears to have developed since the soil temperature survey of Allis and Webber (1984), and now accounts for ~74% (or $53 \pm 4.4 \text{ T/d}$) of the total CO₂ emissions from OHW. Similarly, fractures of up 0.2 m in width have

enhanced heat and mass flow from an area of pre-production thermal ground SE of well BR4 (Fig. 11).

At OHE, comparisons of repeat 1.0 m depth soil temperature surveys indicated no significant changes in the temperature range

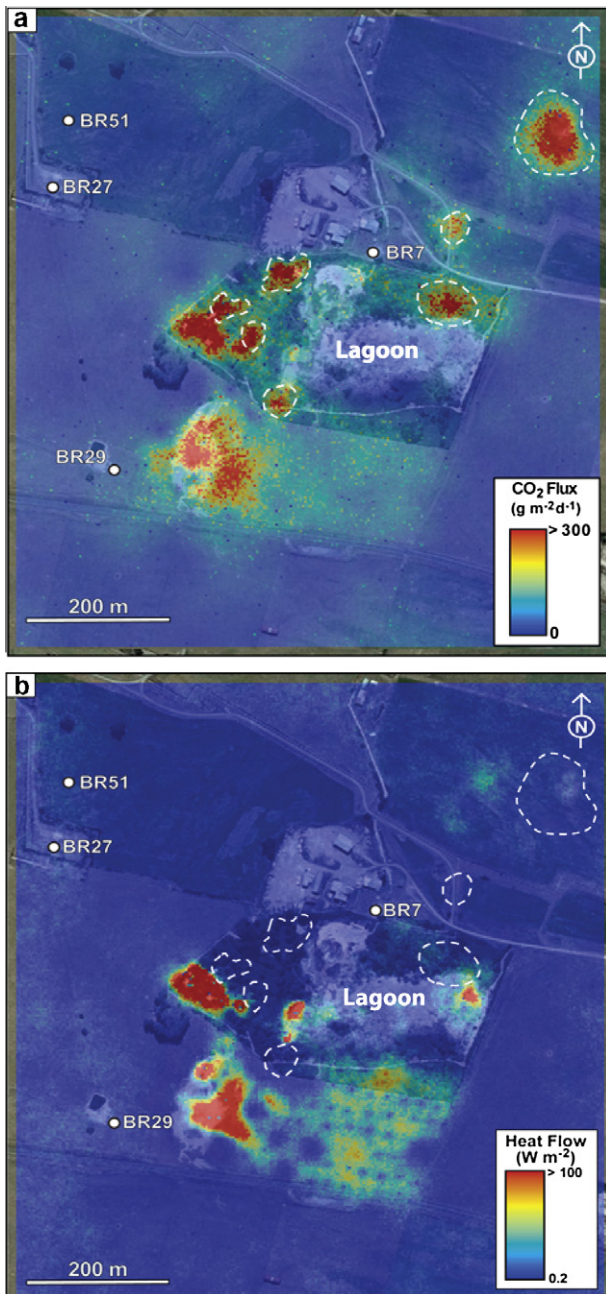


Fig. 10. (a) Pixel plot of sequential Gaussian simulations of diffuse CO_2 flux of the OHE thermal area. (b) Pixel plot of sequential Gaussian simulations of thermal ground heat flow within the OHE thermal area. Note: (i) decoupling of heat flow (white dashed outlines) from CO_2 flux within the NE corner of thermal area and; (ii) minor heat flow and low CO_2 flux across the lagoon area, within which several steam-heated pools and numerous small boiling mud pots occur.

or the extent of thermal ground despite 20 a of production (Thompson, 1967; Allis and Webber, 1984; this study). Well interference testing indicates poor communication between the OHE thermal area and the East Bank reservoir due to the limited permeability of dome lavas (McGuinness, 1985). Well BR7, within the OHE area, was too tight to be productive and abandoned soon after drilling in 1967, resulting in relatively minor mass extraction from the area (Browne and Ellis, 1970; Grindley, 1970). The stability of heat flow at OHE is attributed to the low permeability of dome lavas that effectively shelter this area from production induced effects (mass withdrawal and pressure decline) occurring within the main reservoir. The sheltering of the OHE thermal area by

low permeability lavas is also evident in the absence of any significant ground subsidence across this area (Rissmann, 2010).

On the basis of the long-term thermal stability of OHE, the current heat flow value of 26.7 ± 3 MW is considered a reasonable estimate of the pre-production value. Combining the pre-production heat flow for OHW (95.1 MW) with that of the OHE, a total pre-production heat flow value for the Ohaaki Field of ~ 122 MW is derived (Table 1).

5.2. CO_2 flux and heat flow pathways

Despite the large contribution of alkali-Cl hot water to heat flow this water contributed little to pre-production CO_2 emissions. Adiabatic cooling of the Ohaaki parent fluids (0.75 M CO_2) from 310°C to 98.7°C would deplete the aqueous phase of its CO_2 by $>99\%$. Therefore, $>99\%$ of the dissolved CO_2 would be lost before the alkali-Cl hot waters reached the surface. These calculations are supported by Mahon and Finlayson (1972), who reported a mean total carbonate alkalinity of 0.007 M (~ 310 ppm) for seepages and a slightly higher concentration of 0.015 M (~ 680 ppm) for the Ohaaki Pool likely due to mixing with shallow steam-heated ground waters that overlie the deep upflow. Therefore, little CO_2 has ever been released through the alkali-Cl seepages/springs with pre-production thermal soils constituting the dominant pathway for CO_2 degassing to the atmosphere at OHW. At OHE, the soil zone persists as the dominant ($>99\%$) heat and CO_2 flux pathway, with a minor contribution ($\leq 1\%$ or ~ 0.2 MW; Dickinson, 1967) from the numerous small boiling mud pots and tepid acid-sulphate pools that occur within the lagoon.

In summary, since records began the soil zone has been the dominant pathway for both heat flow and mass flow (CO_2) at Ohaaki. These findings support numerous studies over the last 15 a which indicate the soil zone to be the major pathway for mass and heat transfer from underlying volcanic and hydrothermal reservoirs to the atmosphere (Chiodini et al., 1998; Werner et al., 2000; Favara et al., 2001; Mörner and Etiope, 2002; Fridriksson et al., 2006).

5.3. Relationship of CO_2 flux to reservoir chemistry and upflow zones

The highest flux ($>32,000$ $\text{g m}^{-2} \text{d}^{-1}$), and the greatest numbers of high flux values, were recorded within OHW, which is situated directly above the West Bank upflow where the highest permeabilities exist for rapid transport between the CO_2 source and the surface (Rissmann et al., 2011) and where deep fluids release the greatest proportion of CO_2 due to depressurisation and boiling at depth (Christenson et al., 2002). The spatial overlap between OHW and the West Bank upflow is displayed diagrammatically in Figs. 2 and 12, within which key reservoir metrics of hot fluid upflow (reservoir Cl concentration, reservoir temperature, and N_2/Ar ratios) are contoured from production well data (Hedenquist, 1990; Christenson et al., 2002).

Even though the maximum flux is just $21,200$ $\text{g m}^{-2} \text{d}^{-1}$, the high flux and emission rates of OHE are nevertheless consistent with a direct connection to the East Bank upflow. This view is supported by: (i) the spatial correlation between OHE and maximum Cl concentrations and temperatures from the deep reservoir (Figs. 2 and 12); (ii) elevated N_2/Ar ratios from wells within the area that coincide with elevated N_2/Ar ratios (≥ 300 – air corrected; unpublished data) measured by the authors in steam-heated mud pots, and; (iii) anomalous soil $\text{Hg}_{(v)}$ concentrations (Koga et al., 1982).

Overall the CO_2 flux from the BR6 thermal area is small (mean 24 $\text{g m}^{-2} \text{d}^{-1}$), with just a few small areas of moderately high values (max = 220 $\text{g m}^{-2} \text{d}^{-1}$) detected during transect surveys. Here, at the margins of the field, the underlying aquifers are steam-heated meteoric waters with very high HCO_3^- concentrations

Table 1

Pre-production and current heat flow from surface thermal areas, Ohaaki hydrothermal field. Where N/M = not measured; NN = not naturally occurring, and; D = disappeared due to production.

Source	Location	Steam-heated pools	Thermal ground	Alkali-Cl outflows	Total
<i>Pre-production heat flow (MW)</i>					
Dickinson (1967)	OHW	8.6	25	61.5	95.1
	OHE	<0.2	N/M	NN	<0.2
	BR6	<0.01	<0.1	NN	<0.1
					95.4
<i>Current Heat Flow (MW)</i>					
This study (2010)	OHW	D	43.3 ± 5	D	43.3 ± 5.0
	OHE	N/M	26.7 ± 3	NN	26.7 ± 3.0
	BR6	D	N/M	NN	N/M
					70 ± 6.0
<i>Composite (pre- and current) heat flow (MW)</i>					
Combined	OHW	8.6	25	61.5	95.1
Dickinson (1967)	OHE	<0.2	26.7 ± 3.0	NN	26.9
This study (2010)	BR6	<0.01	<0.1	NN	0.1
					122.1

Table 2

$\delta^{13}\text{CO}_2$ composition, sampling temperature, and flux.

Thermal area	Soil temp. (°C)	CO_2 flux ($\text{g m}^{-2} \text{d}^{-1}$)	$\delta^{13}\text{CO}_2$ (VPDB, ‰)
BR6	14	15	-16.6
OHE	24	34	-7.6
	15	12	-12.5
	98	57	-8.6
	24	92	-5.8
	18	92	-3.8
	40	92	-3.7
	22	120	-4.0
	19	122	-5.9
	34	122	-2.4
	17	153	-2.8
	18	178	-5.9
	20	184	-4.1
	27	184	-3.3
	45	184	-6.8
	45	210	-6.3
	45	210	-6.2
	46	214	-6.4
	25	226	-4.1
	45	301	-6.6
	75	306	-6.9
	17	367	-6.2
	47	367	-5.8
	98	543	-7.9
	70	827	-6.2
	88	1010	-6.0
	95	1225	-6.6
	95	1225	-6.4
OHW	20	15	-10.9
	16	15	-9.0
	99	53	-7.9
	26	61	-6.7
	16	97	-7.2
	56	1227	-7.6
	45	1687	-7.5
	48	2055	-7.8
	86	18,401	-7.1
	91	21,774	-7.6
	91	21,774	-7.6
	99	27,518	-7.0

BR6 = BR6 thermal area; OHE = Ohaaki East thermal area; OHW = Ohaaki West thermal area.

(max = 2284 mg L⁻¹), moderate temperatures (~160 °C) and low-Cl (28 mg L⁻¹) concentrations, which exist within the fractured apex of the East Broadlands Rhyolite (Hedenquist, 1990). The high HCO₃ concentrations of these waters and the absence of a

significant CO₂ flux are consistent with the condensation and solvation, respectively, of a minor mass flux of steam and CO₂, boiled off the deep reservoir, within the cold meteoric groundwaters of the East Broadlands Rhyolite (Hedenquist, 1990; Christenson et al., 2002). A marginal fluid flow regime beneath the BR6 thermal area is consistent with the low CO₂ flux and heat flow detected during the surface survey, and is also supported by the lack of any significant sorbed Hg or free Hg vapour anomaly within the soils of the area (Koga et al., 1982; Murray, 1997).

Importantly, the CO₂ survey supports the conclusions of previous studies on the general upflow patterns of the Ohaaki geothermal system and demonstrates that despite 20 years of production, and a significant decline in reservoir pressure, major CO₂ emission signatures still exist within both major thermal areas. In fact, individual flux rates from OHW and OHE are some of the highest reported for the TVZ (Wardell et al., 2001; Werner et al., 2004; Werner and Cardellini, 2006), and are comparable to values reported for active volcanoes and volcanic hydrothermal systems worldwide (Chiodini et al., 1998; Hernandez et al., 2000; Hernandez et al., 2001; Aiuppa et al., 2004; Bergfeld et al., 2006; Fridriksson et al., 2006; Giannamico et al., 2007).

5.4. Origins and transport of degassed CO₂

The $\delta^{13}\text{CO}_2$ signature of deep production fluids at Ohaaki coincides with the isotopically lighter end of the range of typical mantle values (-6.5 ± 2.5‰; e.g. Nishio et al., 1998), which in conjunction with $\delta^{13}\text{CH}_4$ values, indicates a predominantly magmatic origin for the C, with perhaps a small contribution from organic (kerogen) sources (Christenson et al., 2002).

The isotopic composition of soil gases reflect the transport mechanisms by which the deep gas rises to the surface. During advective gas transport under a pressure gradient the soil zone is saturated with CO₂ and fractionation of the isotopologues ($M^{12}\text{CO}_2$ = 44 and $M^{13}\text{CO}_2$ = 45) does not occur preserving the isotopic signature of the CO₂ source of the underlying reservoir (Capasso et al., 2001; Camarda et al., 2007). This is a common feature of soil gas in hydrothermal and volcanic areas (Natale et al., 2000; Camarda et al., 2007). During diffusive transport a concentration gradient develops and results in accumulation of the ¹³CO₂ molecule in the soil relative to ¹²CO₂, which diffuses at a faster rate (Cerling, 1984; Amundson et al., 1998). This mass bias, or fractionation effect, imparts a characteristic enrichment in subsoil ¹³CO₂ of

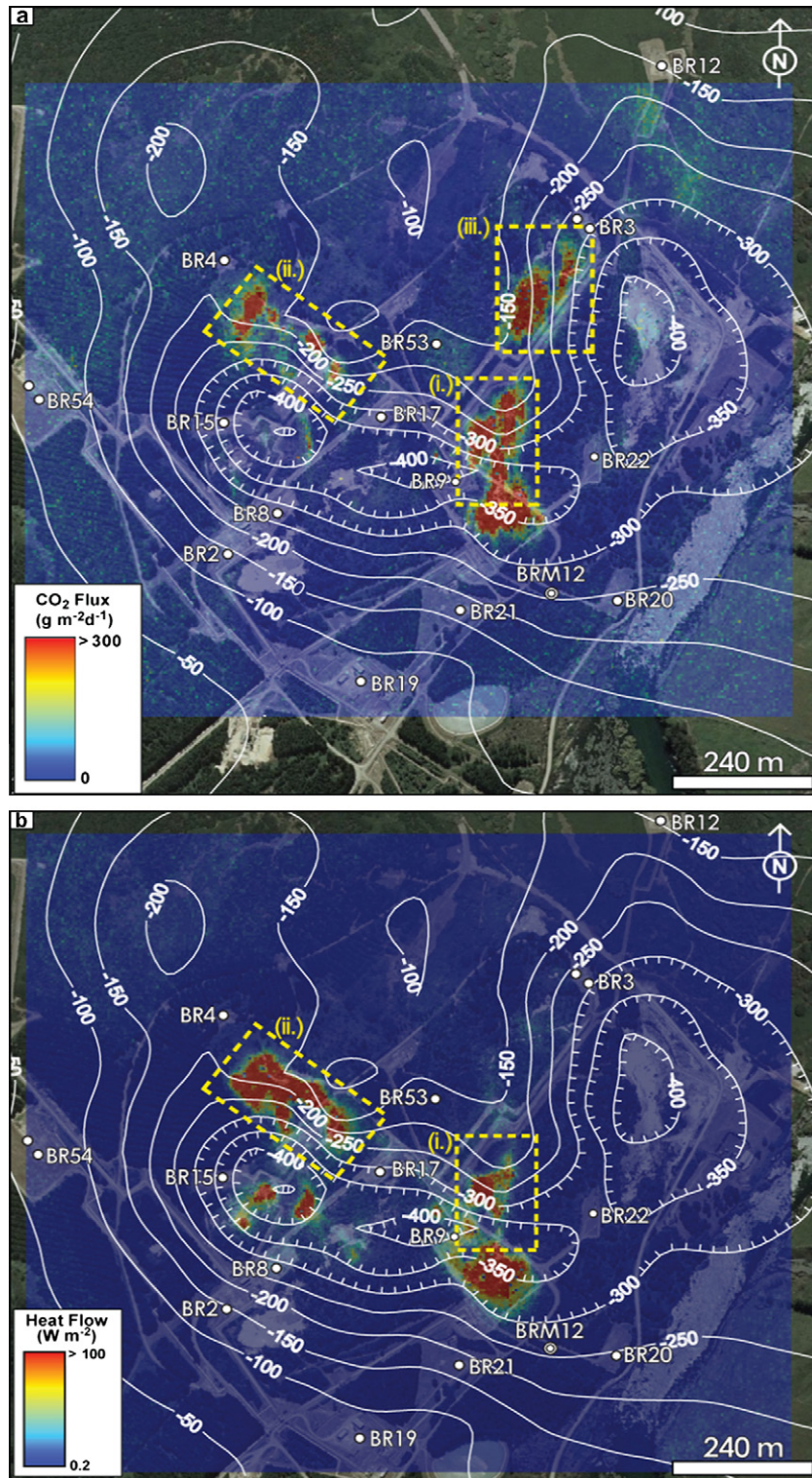


Fig. 11. Overlay of subsidence contours for the Ohaaki West thermal area onto: (a) CO₂ flux, and; (b) heat flux. Note the predominance of CO₂ flux anomalies along zones of maximum tensional strain (where contours are closest – dashed yellow boxes i–iii) as a result of production-induced tensional fracturing due to ground subsidence. (For interpretation of the references to colour in this figure legend, the reader is referred to the web version of this article.)

up to +4.4‰, relative to the isotopic signature of the CO₂ source (Cerling, 1984; Amundson et al., 1998).

The C isotope composition of subsoil CO₂ at high flux sites at OHW and OHE is fairly uniform (Fig. 13), and is similar to the mean composition of West Bank and East Bank bleed-line gas samples, respectively. The subsoil CO₂ is, however, enriched by about

0.9‰ at OHW and 1.8‰ at OHE relative to deep production well fluids, which display few observable differences between the West and East Bank reservoirs (mean $\delta^{13}\text{CO}_2 = -8.3 \pm 0.5\text{\textperthousand}$; Christenson et al., 2002). Christenson et al. (2002) attributed differences in the isotopic composition of bleed-line gases over that of the reservoir to boiling induced precipitation of calcite in the well bore.

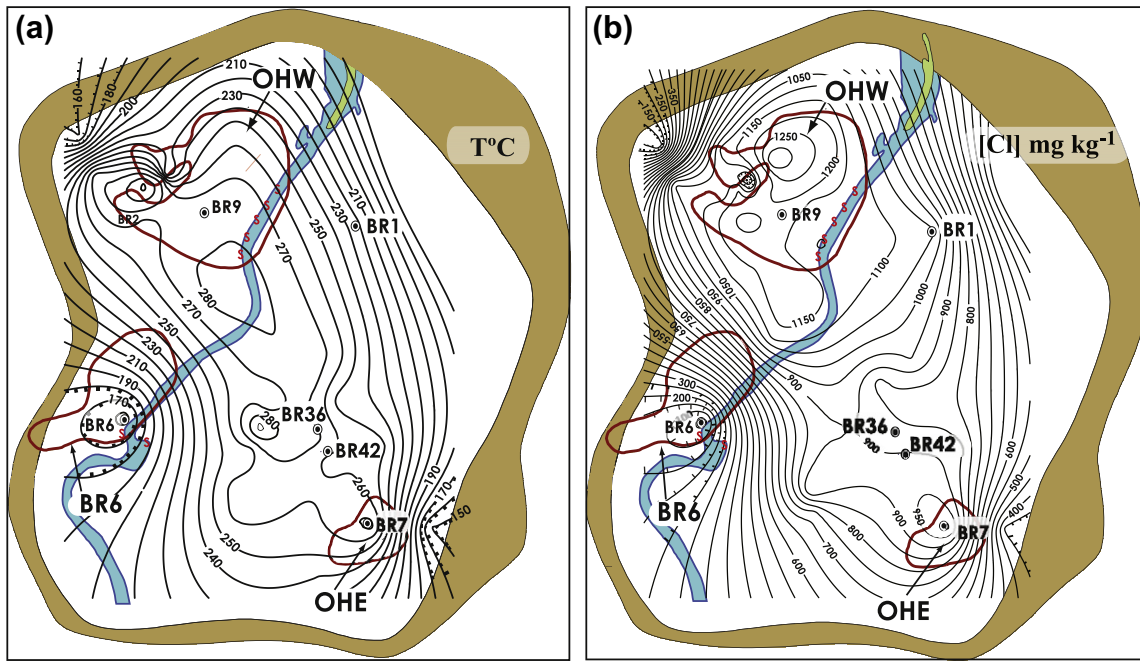


Fig. 12. (a) Contour plot of deep reservoir temperature ($^{\circ}\text{C}$) based on quartz geothermometry, measured enthalpies and measured temperatures for Ohaaki wells (from Hedenquist, 1990). (b) Contour plot of deep reservoir Cl concentration (mg kg^{-1}) corrected for steam loss and excess enthalpy (Hedenquist, 1990).

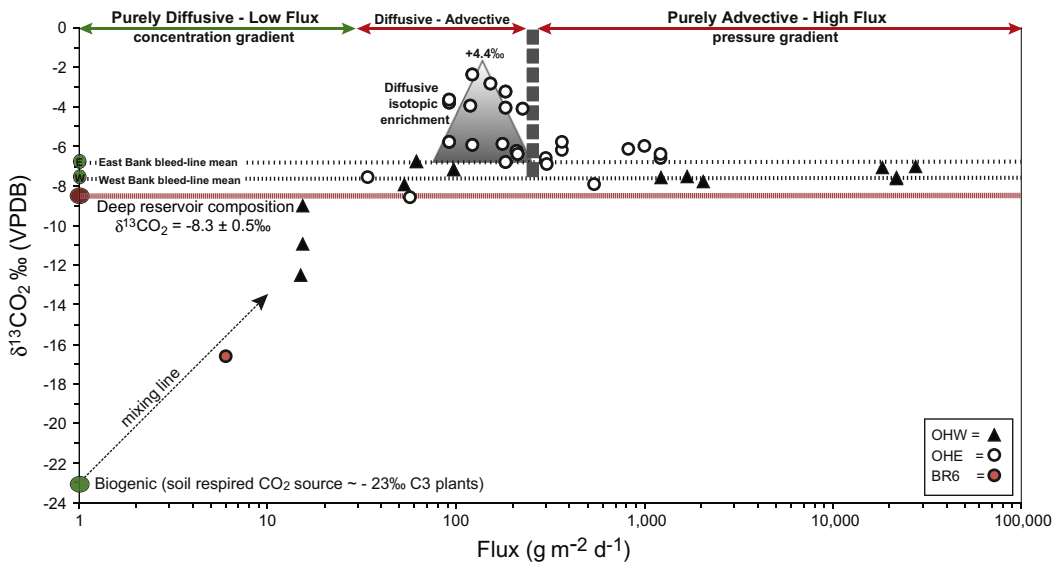


Fig. 13. Plot of $\delta^{13}\text{CO}_2$ soil gas (0.5 m) composition versus CO_2 flux for the OHW and OHE thermal areas. For high flux sites in both thermal areas the $\delta^{13}\text{CO}_2$ composition is similar to that of mean bleed-line gas samples for the West and East Bank reservoirs, representing the boiled magmatic CO_2 source. At low flux rates, $<300 \text{ g m}^{-2} \text{ d}^{-1}$, diffusive fractionation causing isotopic enrichment is important. For fluxes $\leq 15 \text{ g m}^{-2} \text{ d}^{-1}$ the isotopic signatures indicate a contribution from isotopically depleted soil-respired CO_2 . Flux values greater than $15 \text{ g m}^{-2} \text{ d}^{-1}$ exhibit a dominantly hydrothermal signature, as also indicated by a cumulative probability plot of CO_2 flux. Also displayed are flux thresholds by which the mode of gas transport through the soil zone may be defined: (i) $<30 \text{ g m}^{-2} \text{ d}^{-1}$ for purely diffusive gas transport; (ii) between 30 and $300 \text{ g m}^{-2} \text{ d}^{-1}$ for combined diffusive–advective transport, and; (iii) $\geq 300 \text{ g m}^{-2} \text{ d}^{-1}$ for purely advective gas transport.

The present authors also attribute the isotopic enrichment of CO_2 at high-flux sites at OHW and OHE over that of the deep reservoir fluids, to boiling-induced precipitation of calcite during the ascent of magmatic-sourced CO_2 . At OHE the higher non-condensable gas contents of the East Bank reservoir result in more vigorous or longer boiling, and, therefore, proportionately more calcite deposition and ensuing isotopic enrichment (Fig. 13).

The high $\delta^{13}\text{CO}_2$ values and variability of the C isotope composition of low to moderate flux sites suggest that at these sites a two-stage fractionation process characterised by boiling during

fluid ascent within the underlying reservoir, and then isotopic enrichment as CO_2 diffuses through the porous media of the soil zone occurs. The data indicate that over a range of fluxes between 15 and $300 \text{ g m}^{-2} \text{ d}^{-1}$, diffusive and advective transport processes may occur simultaneously (Fig. 13). The highest $\delta^{13}\text{C}$ value at OHE equates to an enrichment of $+4.1\text{\textperthousand}$, indicating nearly pure diffusive gas transport, whereas $\delta^{13}\text{CO}_2$ values for moderate to low flux sites within OHW display no significant diffusive isotopic enrichment. Although the absence of significant diffusive enrichment at OHW may reflect the lack of data over the 100 to

1000 g m⁻² d⁻¹ flux range, they may also result from more direct flow paths related to macro-scale fractures associated with ground subsidence in the area.

Gas transport at Ohaaki is dependent on soil permeability (air-filled porosity and tortuosity), which changes from site to site due to innate heterogeneities of the soil. As such, there is no single CO₂ flux that defines when gas transport changes from purely diffusive to mixed diffusive–advection to purely advective. Instead approximate flux thresholds of <30 g m⁻² d⁻¹ are proposed for purely diffusive gas transport, between 30 and 300 g m⁻² d⁻¹ for combined diffusive–advection transport, and ≥300 g m⁻² d⁻¹ for purely advective gas transport (Fig. 13).

Although a magmatic CO₂ component was evident at all sites, low-temperature sites (<40 °C) with low-flux (<15 g m⁻² d⁻¹) that supported dense stands of non-thermal vegetation also contained a second CO₂ source, most likely from soil-respired (biogenic) CO₂ (−23‰ for C3 plants; Amundson et al., 1998). Those sites with the most depleted isotopic signatures (−12.5‰ to −16.6‰) have soil profiles with well-developed A and B horizons, and decreasing soil temperatures with depth (measured to 1.3 m). Accordingly, isotopic data suggest the threshold at which biogenic soil CO₂ flux constitutes a significant portion of the overall CO₂ flux occurs below ~15 g m⁻² d⁻¹. The background threshold of 15 g m⁻² d⁻¹ is supported by a cumulative probability plot of CO₂ flux data from both thermal areas, with a major inflection occurring at 15 g m⁻² d⁻¹ (Fig. 8). Above the 15 g m⁻² d⁻¹ threshold all isotopic values show an enriched hydrothermal signature whereas below this threshold some contribution from isotopically depleted soil respiration CO₂ is evident (Fig. 13). The biogenic CO₂ signature is likely to decline in concert with increasing soil temperatures and/or CO₂ flux, due to the negative effects of these parameters on vegetation density, and hence biomass accumulation (Gerlach et al., 2001).

6. Conclusions

The total heat flow (122 MW) and CO₂ emissions (111 ± 6.7 T/d) from the Ohaaki hydrothermal system have been quantified for the first time using direct measurement techniques. The CO₂ flux and heat flow survey indicated a net decrease of 52 MW in surface heat flow following 20 a of reservoir production. This decrease in heat flow is associated with the decline of alkali–Cl outflows and steam-heated pools within OHW due to reservoir pressure decline. A post-production increase of 18 MW in thermal ground heat flow at OHW reflects permeability increases associated with production-induced draw down and ground subsidence. By comparison the steam-heated OHE showed no significant change in the extent or vigour of surface thermal activity following 20 a reflecting the role of low permeability lavas in isolating this area from production-induced effects. Based on evidence for the loss of the majority (>98%) of dissolved CO₂ prior to reaching the surface, the large mass flow of alkali–Cl hot waters is unlikely to have contributed significantly to the net CO₂ emissions from the field. Rather, the soil zone at Ohaaki has remained the dominant pathway for CO₂ flux from the underlying reservoir to the atmosphere. The findings indicate that despite 20 a of production the variability in location, spatial extent and magnitude of CO₂ flux remains consistent with established geochemical and geophysical models of the Ohaaki Field.

The chemical and isotopic signature of discharged fluids and gases support the presence of a predominantly magmatic origin for the C. Isotopic data indicate a two-stage fractionation process for sites of moderate CO₂ flux: boiling induced calcite deposition during fluid ascent within the underlying reservoir, and subsequent isotopic enrichment as CO₂ diffuses through the porous media of the soil zone. For high-flux sites the δ¹³CO₂ signature is

unaffected by near-surface (soil zone) fractionation processes, and reflects the composition of the boiled magmatic CO₂ source. Even for low flux sites (<30 g m⁻² d⁻¹) a hydrothermal CO₂ component is evident. Both cumulative probability plots and C isotope signatures of soil gas support a background (atmospheric and soil respiration) CO₂ flux threshold of 15 g m⁻² d⁻¹.

Acknowledgements

We thank the staff of the geothermal group at Contact Energy for access to the Ohaaki Field, logistical and field support and for critical review. Likewise we thank the staff of Wairakei GNS who donated generously of their time and experience and also aided in the maintenance and lease of field equipment, and provided access to detailed cross-sections and historical reports. We acknowledge Deborah Bergfeld and an anonymous party whose reviews greatly improved the quality of this manuscript. Likewise Jerry Fairley, Steve Ingebritsen and Peter Kelly are gratefully acknowledged for comments and technical suggestions. Field assistance was provided by C. Rigg, M. Hughes, P. Chisholm, M. Ohnacker, and M. Fookes. The majority of funding for this project was provided by Contact Energy, with additional support from the Mason Trust Fund of the University of Canterbury.

References

- Aiuppa, A., Caleca, A., Federico, C., Gurrieri, S., Valenza, M., 2004. Diffuse degassing of carbon dioxide at Somma-Vesuvius volcanic complex (Southern Italy) and its relation with regional tectonics. *J. Volcanol. Geotherm. Res.* 133, 55–79.
- Allis, R.G., Webber, S., 1984. Shallow temperature measurements at Wairakei and Broadlands fields. *Geophys. Div. Rep.* 197, 27.
- Amundson, R., Stern, L., Baisden, T., Wang, Y., 1998. The isotopic composition of soil and soil-respired CO₂. *Geoderma* 82, 83–114.
- Bergfeld, D., Evans, W.C., Howle, J.F., Farrar, C.D., 2006. Carbon dioxide emissions from vegetation-kill zones around the resurgent dome of Long Valley Caldera, eastern California, USA. *J. Volcanol. Geotherm. Res.* 152, 140–156.
- Bibby, H.M., Caldwell, T.G., Davey, F.J., Webb, T.H., 1995. Geophysical evidence on the structure of the Taupo volcanic zone and its hydrothermal circulation. *J. Volcanol. Geotherm. Res.* 68, 29–58.
- Brombach, T., Hunziker, J.C., Chiodini, G., Cardellini, C., Marini, L., 2001. Soil diffuse degassing and thermal energy fluxes from the southern Lakki Plain, Nisyros (Greece). *Geophys. Res. Lett.* 28, 69–72.
- Browne, P.R.L., Ellis, A.J., 1970. The Ohaki-Broadlands hydrothermal area, New Zealand; mineralogy and related geochemistry. *Am. J. Sci.* 269, 97–131.
- Camarda, M., De Gregorio, S., Favara, R., Gurrieri, S., 2007. Evaluation of carbon isotope fractionation of soil CO₂ under an advective–diffusive regime: a tool for computing the isotopic composition of unfractionated deep source. *Geochim. Cosmochim. Acta* 71, 3016–3027.
- Capasso, G., D'Alessandro, W., Favara, R., Inguaggiato, S., Parello, F., 2001. Kinetic isotope fractionation of CO₂ carbon due to diffusion processes through the soil. In: Cidu, R. (Ed.), Proc. 10th Internat Symp. Water-Rock Interaction, pp. 1497–1499.
- Cardellini, C., Chiodini, G., Frondini, F., 2003. Application of stochastic simulation to CO₂ flux from soil; mapping and quantification of gas release. *J. Geophys. Res.* 108 (B9), 13.
- Cerling, T.E., 1984. The stable isotopic composition of modern soil carbonate and its relationship to climate. *Earth Planet. Sci. Lett.* 71, 229–240.
- Chiodini, G., Cioni, R., Guidi, M., Raco, B., Marini, L., 1998. Soil CO₂ flux measurements in volcanic and geothermal areas. *Appl. Geochem.* 13, 543–552.
- Chiodini, G., Avino, R., Brombach, T., Caliro, S., Cardellini, C., De Vita, S., Frondini, F., Granieri, D., Marotta, E., Ventura, G., 2004. Fumarolic and diffuse soil degassing west of Mount Epomeo, Ischia, Italy. *J. Volcanol. Geotherm. Res.* 133, 291–309.
- Chiodini, G., Granieri, D., Avino, R., Caliro, S., Costa, A., Werner, C., 2005. Carbon dioxide diffuse degassing and estimation of heat release from volcanic and hydrothermal systems. *J. Geophys. Res.* 110 (B8), 17.
- Christenson, B.W., Mroczeck, E.K., Kennedy, B.M., van Soest, M.C., Stewart, M.K., Lyon, G., 2002. Ohaaki reservoir chemistry: characteristics of an arc-type hydrothermal system in the Taupo volcanic zone, New Zealand. *J. Volcanol. Geotherm. Res.* 115, 53–82.
- Cole, J.W., 1990. Structural control and origin of volcanism in the Taupo volcanic zone. *N. Z. Bull. Volcanol.* 52, 445–459.
- Contact Energy, 2007. Ohaaki well and Stratigraphic, Geochemistry and Pressure Point Database.
- Dawson, G.B., 1964. The nature and assessment of heat flow from hydrothermal areas. *N. Z. J. Geol. Geophys.* 7, 155–171.
- Dawson, G.B., 1988. Broadlands Geothermal Field Environmental Monitoring (Ground Temperature and Geothermal Feature Survey). Report No. 91, Department of Scientific and Industrial Research (D.S.I.R.), Wellington.

- Dawson, G.B., Dickinson, D.J., 1970. Heat flow studies in thermal areas of the North Island of New Zealand. *Geothermics* 2, 466–473.
- Deutsch, C.V., Journel, A.G., 1998. *GSLIB: Geostatistical Software Library and User's Guide*. Applied Geostatistics Series. Oxford University Press, New York, Oxford.
- Dickinson, D.J., 1967. The Natural Heat output of the Broadlands Geothermal Area, 1967. Internal Report [unpublished], Department of Scientific and Industrial Research – Geophysics Division, Wellington.
- Favara, R., Giannanco, S., Inguaggiato, S., Pecorino, G., 2001. Preliminary estimate of CO₂ output from Pantelleria Island volcano (Sicily, Italy): evidence of active mantle degassing. *Appl. Geochem.* 16, 883–894.
- Fridriksson, T., Kristjansson, B.R., Armansson, H., Margaretdottir, E., Olafsdottir, S., Chiodini, G., 2006. CO₂ emissions and heat flow through soil, fumaroles, and steam-heated mud pools at the Reykjanes geothermal area, SW Iceland. *Appl. Geochem.* 21, 1551–1569.
- Gerlach, T.M., Doukas, M.P., McGee, K.A., Kessler, R., 2001. Soil efflux and total emission rates of magmatic CO₂ at the Horseshoe Lake tree kill, Mammoth Mountain, California, 1995–1999. *Chem. Geol.* 177, 101–116.
- Giannanco, S., Parella, F., Gambardella, B., Schifano, R., Pizzullo, S., Galante, G., 2007. Focused and diffuse effluxes of CO₂ from mud volcanoes and mofettes south of Mt. Etna (Italy). *J. Volcanol. Geotherm. Res.* 165, 46–63.
- Giggenbach, W.F., 1995. Variations in the chemical and isotopic composition of fluids discharged from Taupo Volcanic Zone, New Zealand. *J. Volcanol. Geotherm. Res.* 68, 89–116.
- Glover, R.B., Hunt, T.M., Severne, C.M., 2000. Impacts of development on a natural thermal feature and their mitigation; Ohaaki Pool, New Zealand. *Geothermics* 29, 509–523.
- Goovaerts, P., 1997. Kriging vs. stochastic simulation for risk analysis in soil contamination. In: Soares, A., Gómez-Hernández, J., Froidevaux, R. (Eds.), *GeoENV I Geostatistics for Environmental Applications*. Kluwer Academic, Dordrecht, Kluwer, pp. 247–258.
- Grant, M.A., 1977. Broadlands; a gas-dominated geothermal field. *Geothermics* 6, 9–29.
- Grant, M.A., Donaldson, I.G., Bixley, P.F., 1982. *Geothermal Reservoir Engineering*. Academic Press, New York.
- Grindley, G.W., 1970. Subsurface structures and relation to steam production in the Broadlands geothermal field, New Zealand. *Geothermics* 2, 248–261.
- Hedenquist, J.W., 1990. The thermal and geochemical structure of the Broadlands-Ohaaki geothermal system, New Zealand. *Geothermics* 19, 151–185.
- Henrys, S.A., Hochstein, M.P., 1990. Geophysical structure of the Broadlands-Ohaaki geothermal field (New Zealand). *Geothermics* 19, 129–150.
- Hernandez, P.A., Natale, G., Tsunomori, F., Sugiyama, K., Ito, T., Notsu, K., Okada, H., Salazar, J.M., Perez, N.M., 2000. Diffuse emissions of carbon dioxide from Tarumae Volcano, Japan. *Trans. Am. Geophys. Union* 81 (Suppl. 48), 1319.
- Hernández, P.A., Salazar, J.M., Shimoike, Y., Mori, T., Notsu, K., Pérez, N., 2001. Diffuse emission of CO₂ from Miyakejima volcano, Japan. *Chem. Geol.* 177, 175–185.
- Hochstein, M.P., Bromley, C.J., 2005. Measurement of heat flux from steaming ground. *Geothermics* 34, 131–158.
- Hunt, T.M., Bromley, C.J., 2000. Some environmental changes resulting from development of Ohaaki geothermal field, New Zealand. In: Proc. World Geothermal Conf., Kyushu, Japan, pp. 621–626.
- Hunt, T.M., Graham, D.J., 1997. Shallow Ground Temperature and Groundwater Temperature Monitoring at Ohaaki (Broadlands) Geothermal Field. Institute of Geological & Nuclear Sciences, Client Report 72640-C.10 (Client/Consultancy).
- Journel, A.G., 1994. Resampling from stochastic simulations. *Environ. Ecol. Stat.* 1, 63–91.
- Koga, A., Taguchi, S., Mahon, W.A.J., 1982. The use of volatile constituents in geothermal fluids for assessing the type, potential and near surface permeability of a geothermal system; the Broadlands geothermal area, N.Z. In: Proc. Pacific Geothermal Conference, vol. 4. University of Auckland Geothermal Institute, Auckland, pp. 135–138.
- Mahon, W.A.J., Finlayson, J.B., 1972. The chemistry of the Broadlands geothermal area, New Zealand. *Am. J. Sci.* 272, 48–68.
- McGuinness, M.J., 1985. Interference testing of the rhyolites overlying the Ohaaki geothermal reservoir. *Proc. Trans. Geotherm. Resour. Council* 9, 541–545.
- Milichich, S.D., van Dam, M.A., Rosenberg, M.D., Rae, A.J., Bignall, G., 2010. "Earth Research" 3-dimensional geological modelling of geothermal systems in New Zealand: a new visualisation tool. In: Proc. World Geothermal Congress 2010, Bali, Indonesia, 25–30 April 2010. International Geothermal Association, Bali, Indonesia, 7 p.
- Mörner, N.-A., Etiope, G., 2002. Carbon degassing from the lithosphere. *Global Planet. Change* 33, 185–203.
- Murray, K.S., 1997. The use of soil Hg to delineate zones of upwelling in low-to-moderate temperature geothermal systems. *Geothermics* 26, 193–202.
- Natale, G., Hernandez, P., Mori, T., Notsu, K., 2000. Pressure gradient measurements in volcanic diffuse gas emanations. *Geophys. Res. Lett.* 27, 3985–3987.
- Nicol, A., Mazengarb, C., Chanier, F., Rait, G., Uruski, C., Wallace, L., 2007. Tectonic evolution of the active Hikurangi subduction margin, New Zealand, since the Oligocene. *Tectonics* 26, TC4002. doi:10.1029/2006TC002090.
- Nishio, Y., Sasaki, S., Gamo, T., Hiyagon, H., Sano, Y., 1998. Carbon and helium isotope systematics of North Fiji Basin basalt glasses: carbon geochemical cycle in the subduction zone. *Earth Planet. Sci. Lett.* 62, 239–257.
- Rae, A.J., Rosenberg, M.D., Bignall, G., Kilgour, G.N., Milichich, S.D., 2007. Geological results of production well drilling in the western steamfield, Ohaaki geothermal system: 2005–2007. In: Proc. 29th New Zealand Geothermal Workshop, University of Auckland Geothermal Institute.
- Rissmann, C.F., 2010. Using Surface Methods to Understand the Ohaaki Field, Taupo Volcanic Zone, New Zealand. Unpubl. Doctoral Dissertation. Univ. Canterbury, Christchurch, New Zealand.
- Rissmann, C., Nicol, A., Cole, J., Kennedy, B., Fairley, J., Christenson, B., Leybourne, M., Milichich, S., Ring, U., Gravley, D., 2011. Fluid flow associated with silicic lava domes and faults, Ohaaki hydrothermal field, New Zealand. *J. Volcanol. Geotherm. Res.* 204, 12–26.
- Rowland, J.V., Sibson, R.H., 2004. Structural controls on hydrothermal flow in a segmented rift system, Taupo volcanic zone, New Zealand. *Geofluids* 4, 259–283.
- Sorey, M.L., Grant, M.L., Bradford, E., 1980. Nonlinear effects in two-phase flow to wells in geothermal reservoirs. *Water Resour. Res.* 16, 767–777.
- Stratford, W.R., Stern, T.A., 2006. Crust and upper mantle structure of a continental backarc, central North Island, New Zealand. *Geophys. J. Int.* 166, 469–484.
- Thompson, G.E.K., 1967. Ground Temperatures at a Depth of One Metre. Unpublished Report, Department of Scientific and Industrial Research–Geophysics Division, Wellington, New Zealand.
- Wardell, L.J., Kyle, P.R., Dunbar, N., Christenson, B., 2001. White Island volcano, New Zealand: carbon dioxide and sulfur dioxide emission rates and melt inclusion studies. *Chem. Geol.* 177, 187–200.
- Welles, J.M., Demetriades-Shah, T.H., McDermitt, D.K., 2001. Considerations for measuring ground CO₂ effluxes with chambers. *Chem. Geol.* 177, 3–13.
- Werner, C., Cardellini, C., 2006. Comparison of carbon dioxide emissions with fluid upflow, chemistry, and geologic structures at the Rotorua geothermal system, New Zealand. *Geothermics* 35, 221–238.
- Werner, C., Brantley, S.L., Boomer, K., 2000. CO₂ emissions related to the Yellowstone volcanic system. 2. Statistical sampling, total degassing, and transport mechanisms. *J. Geophys. Res.* 105, 10,831–10,846.
- Werner, C., Hochstein, M.P., Bromley, C.J., Manville, V.R., Tilyard, D., 2004. CO₂-flux of steaming ground at Karapiti (Wairakei, NZ). *Geol. Soc. N. Z.* 117A, 115–116.
- White, P.J., Lawless, J.V., Terzaghi, S., Okada, W., 2005. Advances in subsidence modelling of exploited geothermal fields. In: Proc. World Geothermal Conference, Antalya, Turkey.
- Wilson, C.J.N., Houghton, B.F., McWilliams, M.O., Lanphere, M.A., Weaver, S.D., Briggs, R.M., 1995. Volcanic and structural evolution of Taupo volcanic zone, New Zealand: a review. *J. Volcanol. Geotherm. Res.* 68, 1–28.
- Wood, C.P., 1994. The Waiora Formation geothermal aquifer, Taupo volcanic zone, New Zealand. In: Proc. 16th New Zealand Geothermal Workshop, University of Auckland Geothermal Institute, pp. 121–126.
- Wood, C.P., Brathwaite, R.L., Rosenberg, M.D., 2001. Basement structure, lithology and permeability at Kawerau and Ohaaki geothermal fields, New Zealand. *Geothermics* 30, 461–481.